Electronic Supplementary Material (ESI) for Organic & Biomolecular Chemistry

On the Role of Guests in Enforcing the Mechanism of Action of Gated Baskets

Yian Ruan, Bao-Yu Wang, Jeremy M. Erb, Shigui Chen, Christopher M. Hadad, and Jovica D. Badjic*

The Ohio State University, 100 W. 18th Avenue, Columbus OH 43210, USA.
E-mail: badjic@chemistry.ohio-state.edu

SUPPLEMENTARY INFORMATION

General information

All chemicals were purchased from commercial sources, and used as received unless stated otherwise. All solvents were dried prior touse according to standard literature procedures. Chromatography purifications were performed using silica gel 60 (Sorbent Technologies 40-75µm, 200 x 400mesh). Thin-layer chromatography (TLC) was performed on silica-gel plate w/UV254 (200µm).Chromatograms were visualized by UV-light and stained using 20% phosphomolybdic acid in ethanol if needed. All NMR samples were prepared in J. Young Valve NMR Tubes purchased from Norell. ^{1}H and ^{13}C NMR spectra were recorded, at 400 MHz or 500 MHz and 100 MHz or 125 MHz respectively, on a Bruker DPX-400 spectrometerunless otherwise noted.They were referenced using the solvent residual signal as an internal standard. NMR samples were prepared using $CDCl_3$, $CD_2Cl_2$and Methanal-d4 purchased from Cambridge Isotope Laboratories. The chemical shift values are expressed as δ values (ppm) and the couple constants values (J) are in Hertz (Hz). The following abbreviations were used for signal multiplicities: s, singlet; d, doublet; t, triplet; m, multiplet; and br, broad. For NMR measurement, temperatures were corrected with neat methanol standard. ^{1}HRMS (ESI) were measured on a Micromass Q-TofII spectrometer.

Synthesis

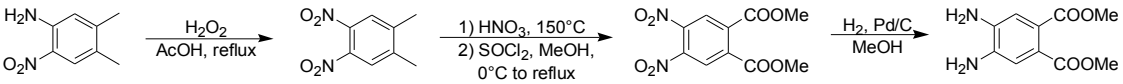

Scheme S1. Compound **6** was prepared in accord with literature procedures[1-3] with spectroscopic data in agreement with those reported previously: ^{1}H NMR (500 MHz, $CDCl_3$, 300 K): δ (ppm) = 6.99 (s, 2H), 3.83 (s, 6H); ^{13}C NMR (125 MHz, $CDCl_3$, 300 K): δ (ppm) = 168.4, 136.7, 123.9, 116.5, 52.3.

Compound 7: To a solution of 5-norbornene-2,3-dione **5** (2.00 g, 0.0164 mol)[4] in DCM (25.0 ml) was added 4,5-diamino-phthalic acid dimethyl ester **6** (3.67 g, 0.0164 mol). The reaction was allowed to stir for 3 h and then the solvent was removed under reduced pressure. The crude product was purified by column chromatography (SiO_2; hexanes: EtOAc = 5:3) to afford **7** as a light-yellow solid (4.67 g, 92%).^{1}H NMR (500 MHz, $CDCl_3$, 300 K): δ (ppm) = 8.23 (s, 2H), 6.87 (s, 2H), 3.98 (s, 2H), 3.94 (s, 6H), 2.78 (d, 1H, J = 9 Hz), 2.58 (d, 1H, J = 9 Hz); ^{13}C NMR (125 MHz, $CDCl_3$, 300 K): δ (ppm) = 168.9, 167.3, 142.2, 139.7, 131.3, 130.0, 62.5, 52.8, 49.4; HRMS ESI: m/z calcd for $C_{17}H_{14}N_2O_4$: 333.0851 $[M+Na]^+$, found: 333.0867.

Compound 8: To a solution of compound **7** (360 mg, 1.16 mmol) in benzene (25.0 mL) was slowly added a solution of bromine (186 mg, 1.16 mmol) in benzene (3.0 mL). The mixture was stirred for 15 min and then concentrated under vacuum to give dibromo product. To a solution of dibromide (400 mg, 0.85 mmol) in DMF (5.0 mL) was added DBU (320 µL, 2.13 mmol). The solution was heated to 90˚C for 5 h. The

mixture was concentrated and partitioned between 80 mL of 6 M NaOH solution and 80 mL of DCM. The aqueous layer was extracted with DCM (3 x 80 mL). The combined organic layers were dried over Na_2SO_4 and concentrated. The crude product was purified by column chromatography (SiO_2; hexanes:EtOAc = 2:1) to give **8** as a white solid (245 mg, 60%).^{1}H NMR (400 MHz, $CDCl_3$, 300 K): δ (ppm) = 8.32 (s, 1H), 8.26 (s, 1H), 6.88 (d, 1H, *J* = 3.3 Hz), 4.04 (m, 1H), 3.96 (s, 7H), 3.02 (d, 1H, *J* = 9 Hz), 2.64 (d, 1H, *J* = 9 Hz); ^{13}C NMR (100 MHz, $CDCl_3$, 300 K): δ (ppm) = 167.3, 167.2, 166.8, 166.6, 140.0, 139.8, 139.6, 134.8, 131.8, 131.6, 130.4, 130.1, 61.8, 57.2, 52.9, 50.9; HRMS ESI: *m*/*z* calcd for $C_{17}H_{13}BrN_2O_4$: 410.9956 $[M+Na]^+$, found: 410.9955.

Compound 9: To a solution of solution of diisopropylamine (0.15 ml, 1.06 mmol) in dry THF (5.0 mL) at -78˚C was added *n*-butyllithium (0.63 ml, 1.6 M in hexane) under an atmosphere of argon. The reaction mixture was stirred for 1 h, and a solution of compound **8** (420 mg, 1.06 mmol) in THF (3.0 mL) was added dropwise over 5 min. The resulting mixture was stirred for an additional 30 min before trimethyltinchloride (215 mg, 1.06 mmol) in THF (2.0 mL) was added. After 2 h at -78˚C, the reaction mixture was gradually warmed to room temperature, washed with water (15 mL), and extracted with diethyl ether (3 x 50mL). The combined organic phase was dried over Na_2SO_4 and concentrated under reduced pressure. The crude product was purified by column chromatography (SiO_2; hexanes:EtOAc = 3:1) to give **9** as a white solid (405 mg, 68%).^{1}H NMR (400 MHz, $CDCl_3$, 300 K): δ (ppm) = 8.30 (s, 1H), 8.26 (s, 1H), 4.08 (d, 1H, *J* = 4 Hz), 3.96 (s, 7H), 2.93 (d, 1H, *J* = 8 Hz), 2.60 (d, 1H, *J* = 8 Hz), 0.26 (s, 9H); ^{13}C NMR (100 MHz, $CDCl_3$, 300 K): δ (ppm) = 167.4, 154.2, 145.3, 140.2, 139.9, 131.5, 131.3, 130.4, 130.1, 61.0, 59.2, 56.0, 52.9, -9.1; HRMS ESI: *m*/*z* calcd for $C_{20}H_{21}BrN_2O_4Sn$: 574.9604 $[M+Na]^+$, found: 574.9616.

Table S1. The cyclotrimerization of **9** (0.18 M) was attempted under various catalytic conditions to in dry DMF (0.5 mL) give diastereomeric $\mathbf{10}_{syn}$ *and* $\mathbf{10}_{anti}$.

	Pd catalyst	Cu Salt	inorganic component (molar equiv)	**10** yield (%)	**10** *syn/anti*
1	$Pd(PPh_3)_4$ (10 %)	CuI (50%)	CsF (2.0)	60	1:3
2	$Pd(PPh_3)_4$ (10 %)	CuI (20%)	CsF (2.0)	20	1:3
3	$PdCl_2$ (10 %)	CuI (20%)	CsF (2.0) $CsClO_4$ (8.0)	0	
4	$Pd(PPh_3)_4$ (10 %)	CuI (20%)	CsF (2.0) $CsClO_4$ (8.0)	0	
5	$Pd(PPh_3)_4$ (10 %)	CuI (20%)	CsF (2.0) CF_3COOAg (2.0)	0	
6		$Cu(NO_3)_2$		0	

Compound $\mathbf{10}_{syn}$: To a solution of **9** (0.050 g, 0.090 mmol) in anhydrous DMF (0.5 mL) at room temperature and under an atmosphere of argon, was added cesium fluoride (27 mg, 0.18 mmol), copper (I) iodide (8.5 mg, 0.045 mmol), and $Pd(PPh_3)_4$ (10.4 mg, 0.009 mmol). The reaction mixture was stirred at 298 K for 17h. The mixture was partitioned between ethyl acetate (20 mL) and water (10 mL) and the aqueous layer was extracted with ethyl acetate (3 x 20 mL). The combined organic layer was dried over Na_2SO_4 and concentrated under reduced pressure. The resulting solid was purified by column

chromatography (SiO_2; EtOAc) to yield the **10**$_{syn}$ as a colorless solid (3.5 mg, 12%). ^{1}H NMR (400 MHz, $CDCl_3$, 300 K): δ (ppm) = 8.16 (s, 6H), 4.73 (s, 8H), 3.90 (s, 18H), 2.99 (d, 3H, J = 9.4 Hz), 2.87 (d, 1H, J = 9.4 Hz); ^{13}C NMR (100 MHz, $CDCl_3$, 300 K): δ (ppm) = 167.1, 165.4, 140.3, 138.6, 131.6, 130.2, 60.8, 52.8, 49.2; HRMS ESI: m/z calcd for $C_{51}H_{36}N_6O_{12}$: 947.2289 $[M+Na]^+$, found: 947.2298

Compound 11: To a solution of **10**$_{syn}$ (10.0 mg, 0.011 mmol) in THF (4.0 mL) was added lithium hydroxide monohydrate (20.0 mg, 0.476 mmol) in H_20 (5.0 ml). The mixture was heated to 80°C for 2 h. THF was removed under reduced pressure and 2 M HCl was added until the solution was acidic (litmus paper). Solid precipitate was collected by centrifuge and dried under vacuum to give hexacid (7.1 mg, 78%). ^{1}H NMR (400 MHz, DMSO-d_6, 300 K): δ (ppm) =8.51 (s, 6H), 4.92 (s, 6H), 2.88 (s, 6H); ^{13}C NMR (100 MHz, DMSO-d_6, 300 K): δ (ppm) =166.9, 165.6, 139.3, 138.3, 60.8, 48.3 ppm; HRMS ESI: m/z calcd for $C_{45}H_{24}N_6O_{12}$: 839.1379 $[M-H]^-$, found: 839.1408.To a mixture of hexacid (7.1 mg, 0.0083 mmol) in toluene (3.0 mL) was added trifluoroacetic anhydride (35.3 µL, 0.25 mmol) at 0°C. After 1 h, the solvent was removed to afford **11** as a white solid (6.2 mg, 95%). ^{1}H NMR (400 MHz, DMSO-d_6, 300 K): δ (ppm) = 8.43 (s, 6H), 5.04 (s, 6H), 3.04 (m, 6H); the solubility of **12** in a variety of solvents as well as chemical stability was low limiting its additional spectroscopic characterization.

Compound 2: To a solution of diamine **12**[5] (3.4 mg, 0.028 mmol) in DMSO (1.0 mL) was added *tris*-anhydride **11** (6.2mg, 0.0079 mmol). Pyridine (0.1 mL) was added before the reaction mixture was heated at 120°C for 10 h. Following, the solvent was removed under reduced pressure and the crude product purified by preparative TLC (SiO_2; DCM:MeOH = 5:1) to give corresponding *tris*-amine as a white solid (4.1 mg, 48%).^{1}H NMR (400 MHz, MeOH-d_4:$CDCl_3$= 1:2, 300 K): δ(ppm) =8.18 (s, 6H), 7.90 (m, 3H), 7.88, (m, 3H), 7.00 (m, 3H), 4.74 (s, 6H), 4.70 (s, 6H), 3.02 (d, 3H, J = 9.6 Hz), 2.92 (d, 3H, J = 9.6 Hz). To a solution of *tris*-amine(4.1 mg, 0.0037 mmol) and triethylamine (10 µL, 0.072 mmol) in dry THF was added trifluoroacetic anhydride (5 µL, 0.035 mmol) at 0°C. The reaction mixture was stirred for 15 min before quenched with H_2O (1.0 mL). THF was removed under vacuum and the mixture partitioned between DCM (5.0 mL) and saturated $NaHCO_3$ solution (5.0 mL). After, the aqueous layer was additionally extracted withDCM (3 x 5.0 mL) and the combined organic layers were dried over Na_2SO_4 and then concentrated under reduced pressure. The crude product was purified by preparative TLC (SiO_2; DCM:MeOH = 15:1) to give **2** as a white solid (4.4 mg, 85%).^{1}H NMR (400 MHz, $CDCl_3$, 300 K): δ (ppm) =11.91 (s, 3H), 8.48 (m, 3H), 8.45, (m, 3H), 8.40 (m, 3H), 8.13 (s, 6H), 4.94 (s, 6H), 4.71 (s, 6H), 3.01 (d, 3H, J = 9.6 Hz), 2.93 (d, 3H, J = 9.6 Hz); ^{13}C NMR (100 MHz, $CDCl_3$, 300 K): δ (ppm) = 165.9, 165.7, 143.2, 142.3, 139.1, 138.9, 130.3, 125.7, 61.2, 53.5, 49.3; HRMS ESI: m/z calcd for $C_{69}H_{38}F_9N_{15}O_9$: 695.6417 $[M+2H]^{2+}$, found: 695.6415.

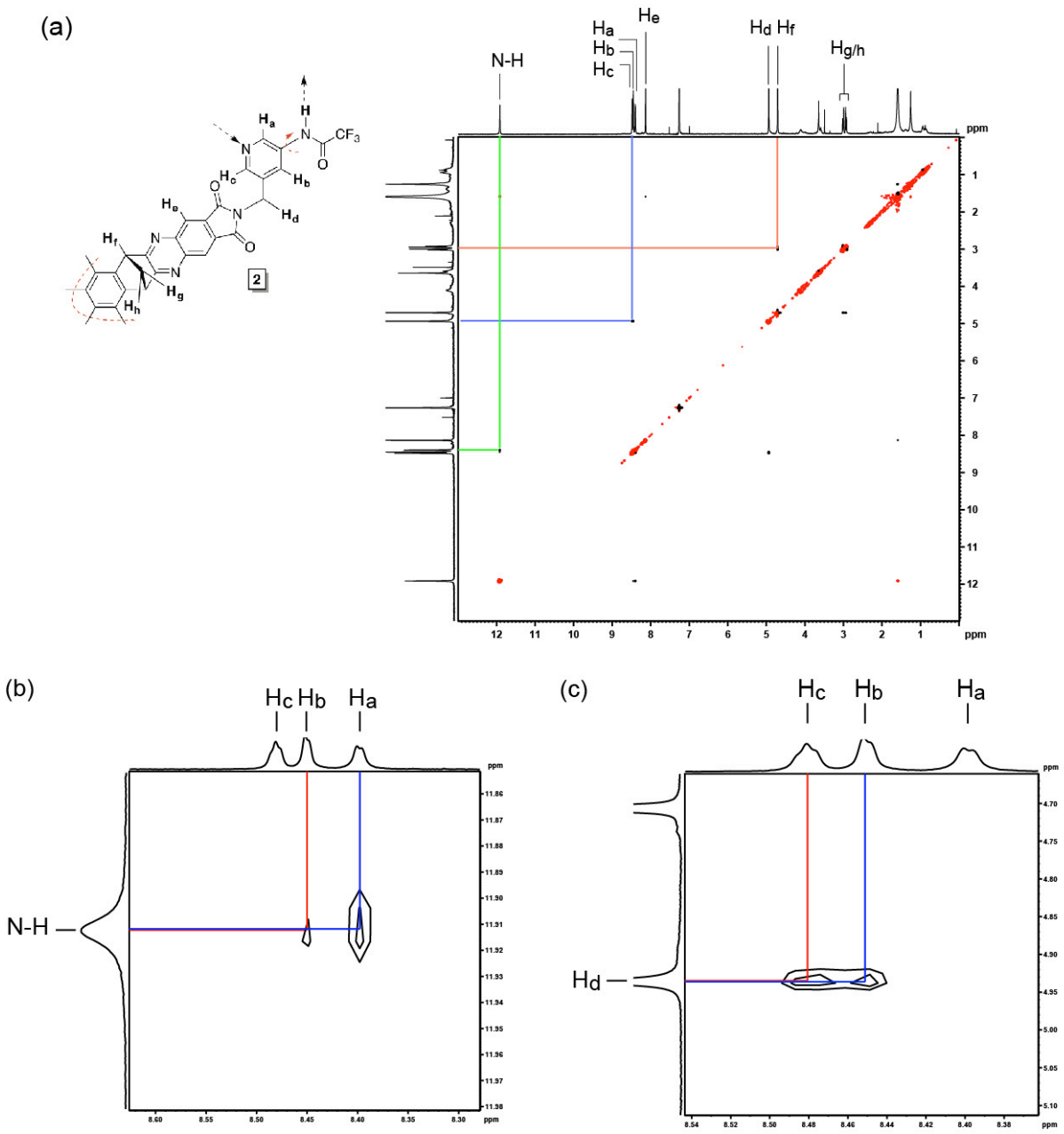

Figure S1. ^{1}H-^{1}H NOESY NMR spectrum (400 MHz) of compound **2** (0.8mM) in $CDCl_3$ at 298.0 K; the number of scans was set to 4.0 while the mixing time τ= 300.0 ms.

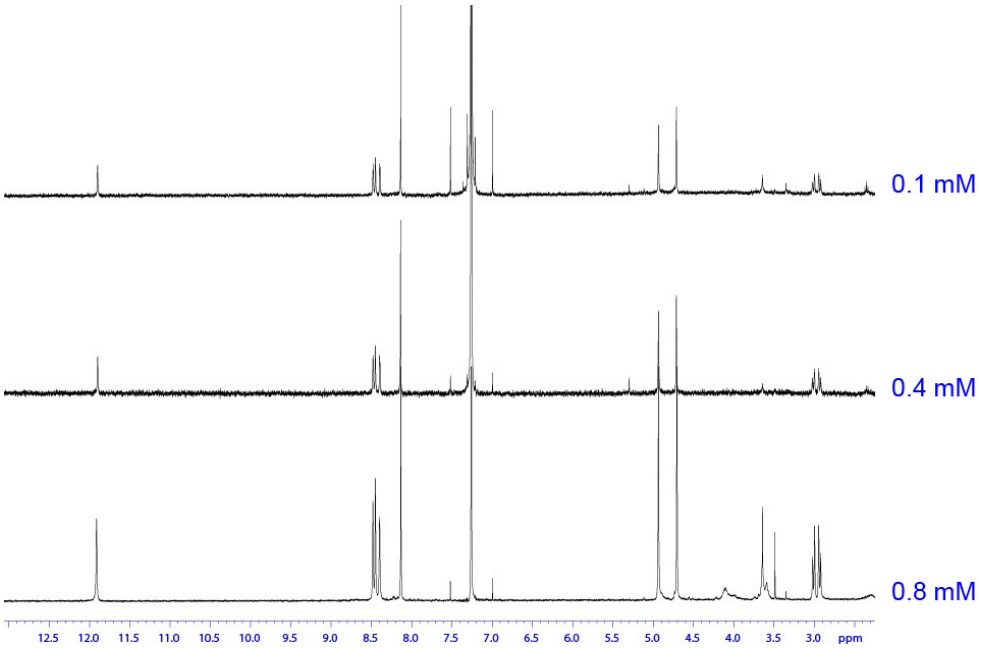

Figure S2. ^{1}H NMR spectra (400 MHz) of variously concentrated solutions of basket **2** (see on the right) in $CDCl_3$ at 298.0 K.

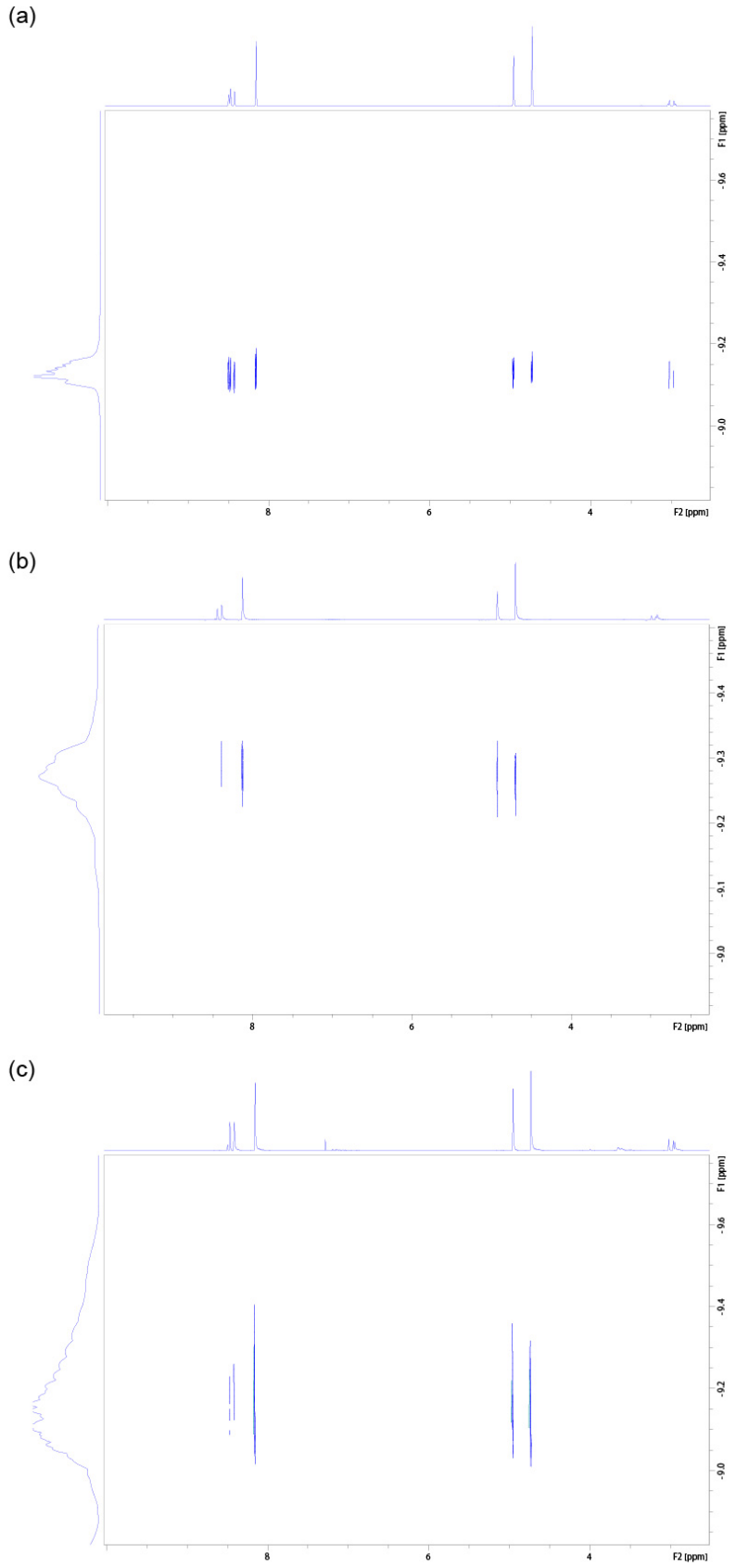

Figure S3. DOSY NMR spectra (400 MHz, 298.0 K) of variously concentrated solutions of basket **2** in $CDCl_3$: (a) 0.8 mM; (b) 0.5 mM; (c) 0.3 mM.

Table S2. Diffusion coefficients and hydrodynamic radii of basket **2** in $CDCl_3$at 298.0 K were obtained from the NMR DOSY measurements.

Concentration mM	Diffusion coefficient (m^2/s)	Hydrodynamic radius Å
0.8	$7.4*10^{-10}$	5.4
0.5	$5.5*10^{-10}$	7.3
0.3	$6.5*10^{-10}$	6.2

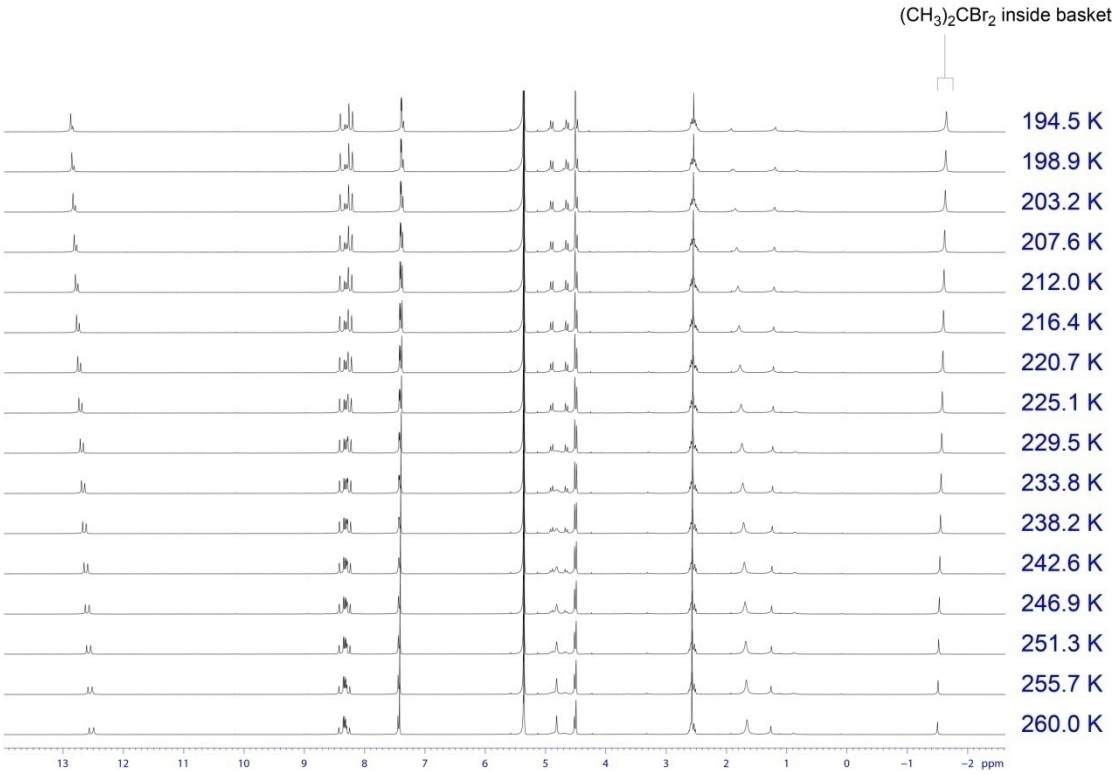

Figure S4. Variable temperature ^1H NMR spectra (400 MHz) of basket **1** (2.6mM) containing 1.25 molar equivalents of dibromopropane in CD_2Cl_2.

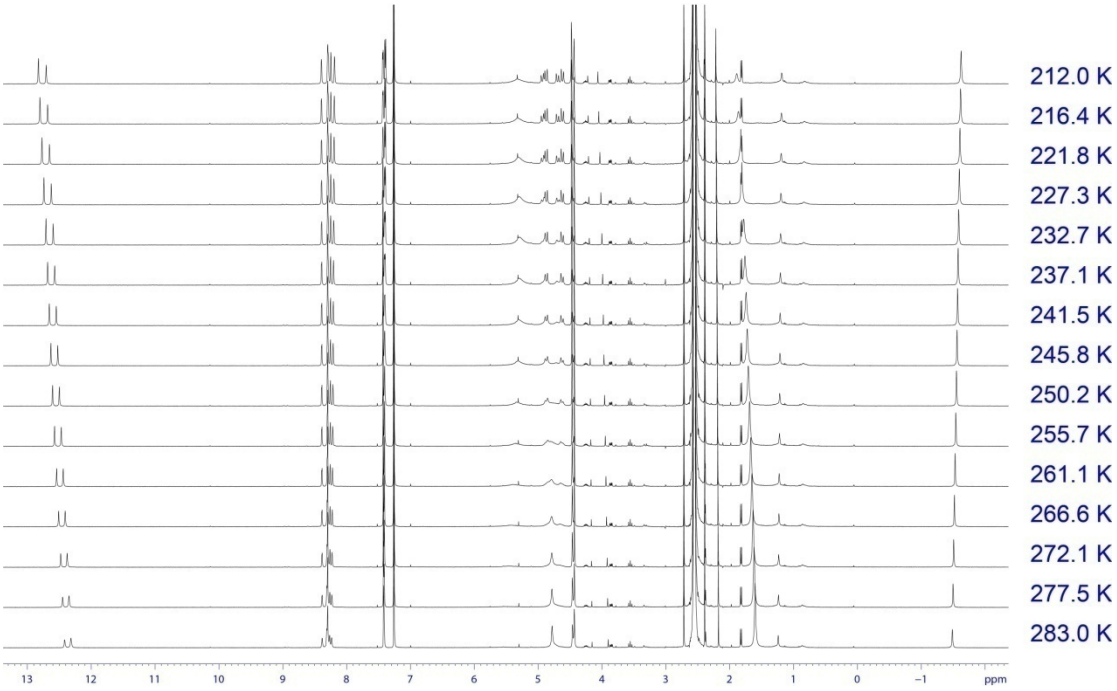

Figure S5. Variable temperature ^{1}H NMR spectra (400 MHz) of basket **1** (2.0 mM) containing 85.0 molar equivalents of dibromopropane in $CDCl_3$.

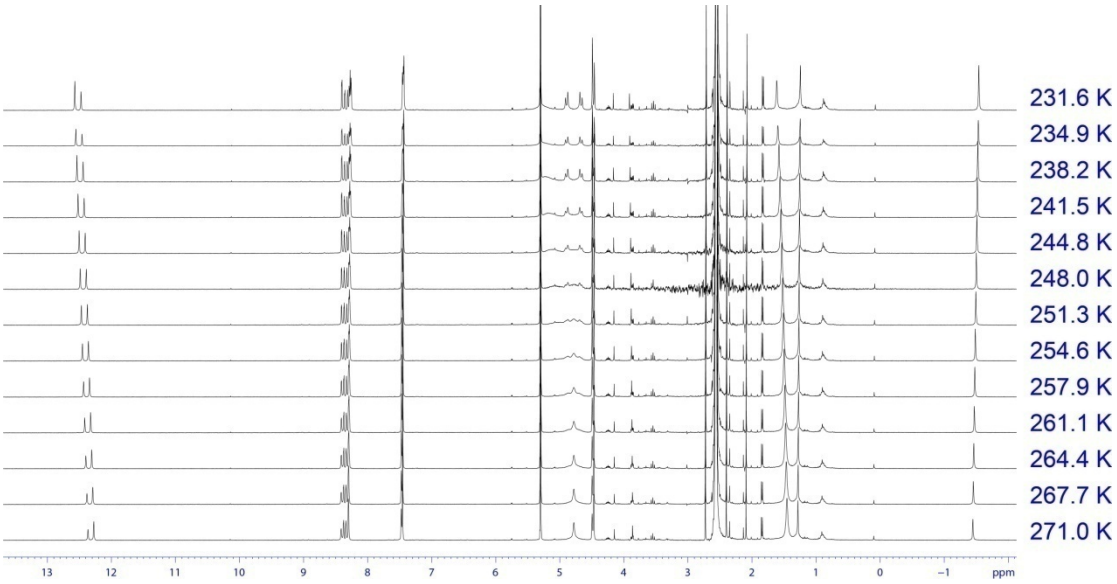

Figure S6. Variable temperature ^{1}H NMR spectra (400 MHz) of basket **1** (1.9 mM) containing 81.0 molar equivalents of dibromopropane in $CFCl_3/CD_2Cl_2$ = 7:3.

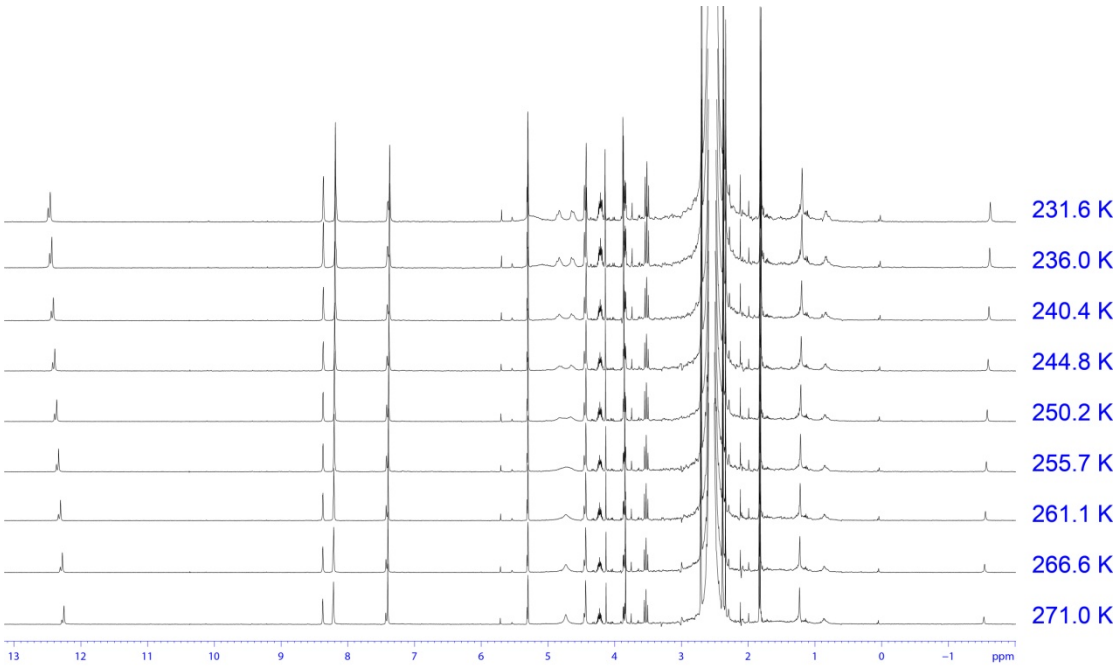

Figure S7. Variable temperature ^{1}H NMR spectra (400 MHz) of basket **1** (1.9 mM) containing 1000 molar equivalents of dibromopropane in CCl_4:CD_2Cl_2 = 8:2.

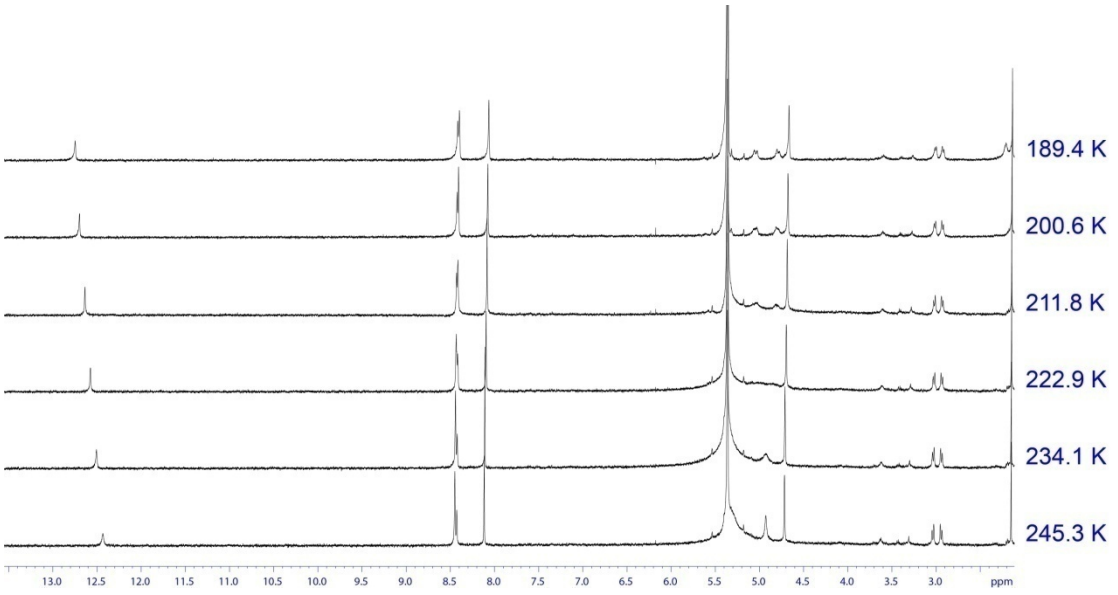

Figure S8. Variable temperature ^{1}H NMR spectra (500 MHz) of basket **2** (0.50 mM) containing 470.0 molar equivalents of hexachloroethane in CD_2Cl_2.

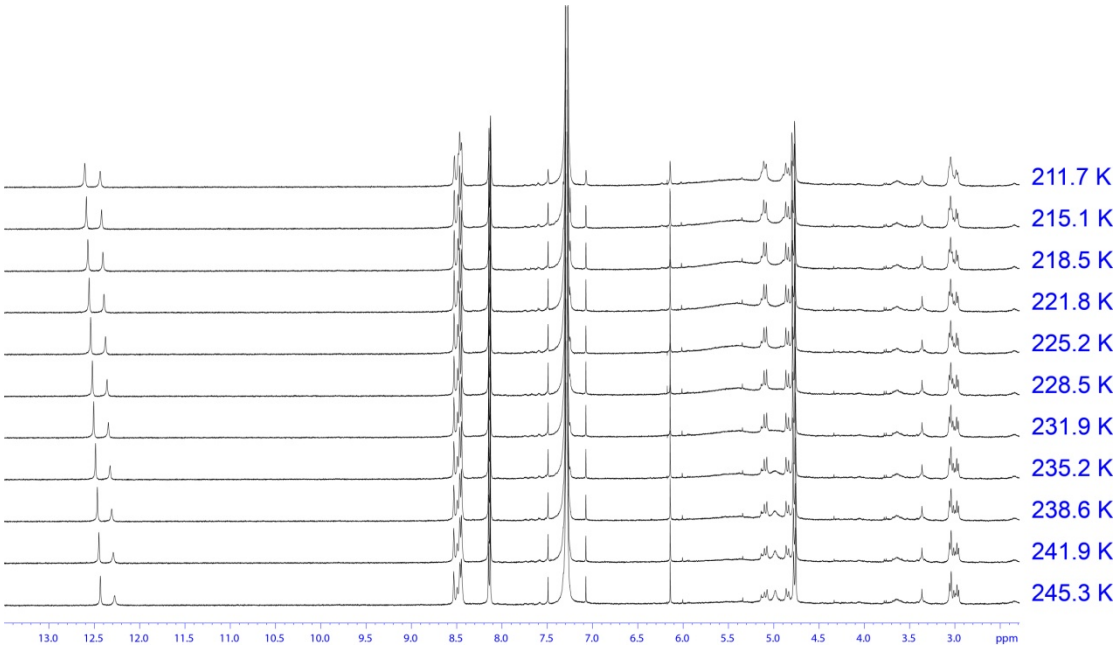

Figure S9. Variable temperature ^{1}H NMR spectra (500 MHz) of basket **2** (0.27 mM) containing 553.0 molar equivalents of hexachloroethane in $CDCl_3$.

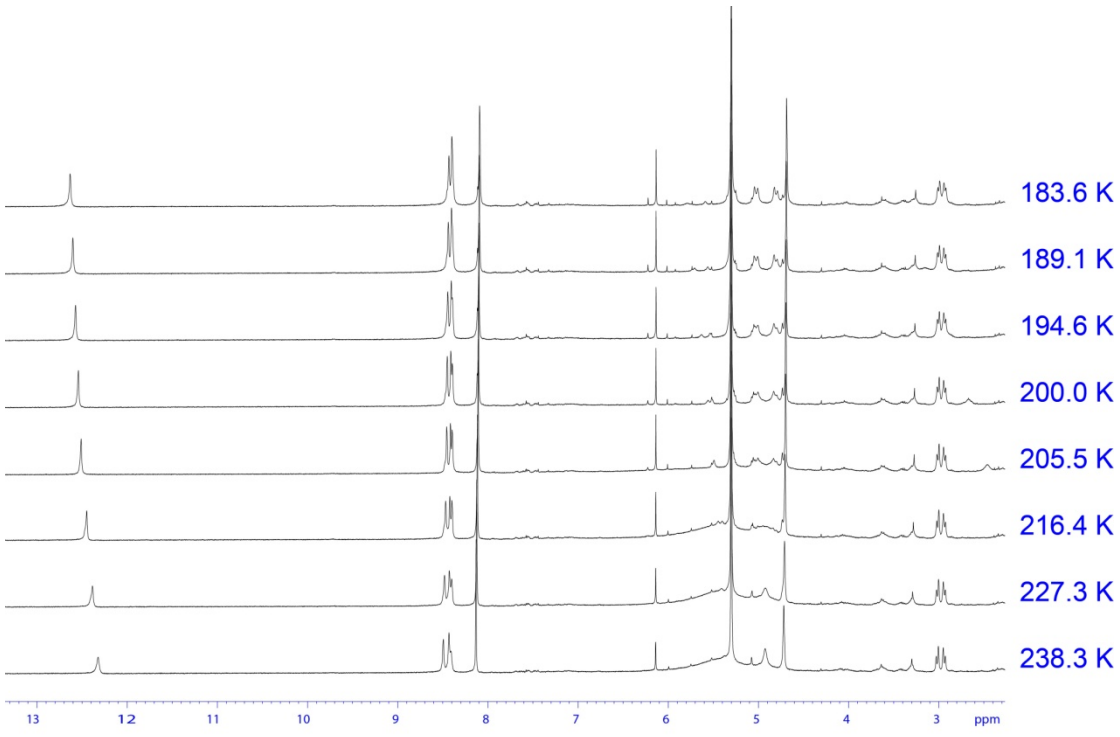

Figure S10. Variable temperature ^{1}H NMR spectra (400 MHz) of basket **2** (0.50 mM) containing 470.0 molar equivalents of hexachloroethane in $CFCl_3/CD_2Cl_2$ = 7:3.

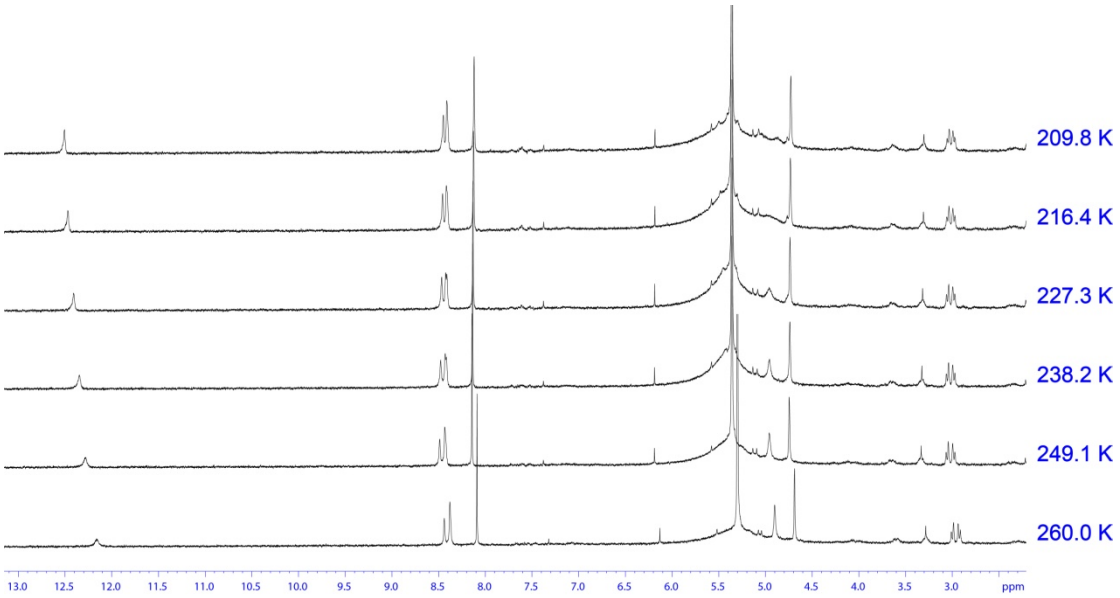

Figure S11. Variable temperature ^{1}H NMR spectra (400 MHz) of basket **2** (0.50 mM) containing 470.0 molar equivalents of hexachloroethane in CCl_4/CD_2Cl_2= 8:2.

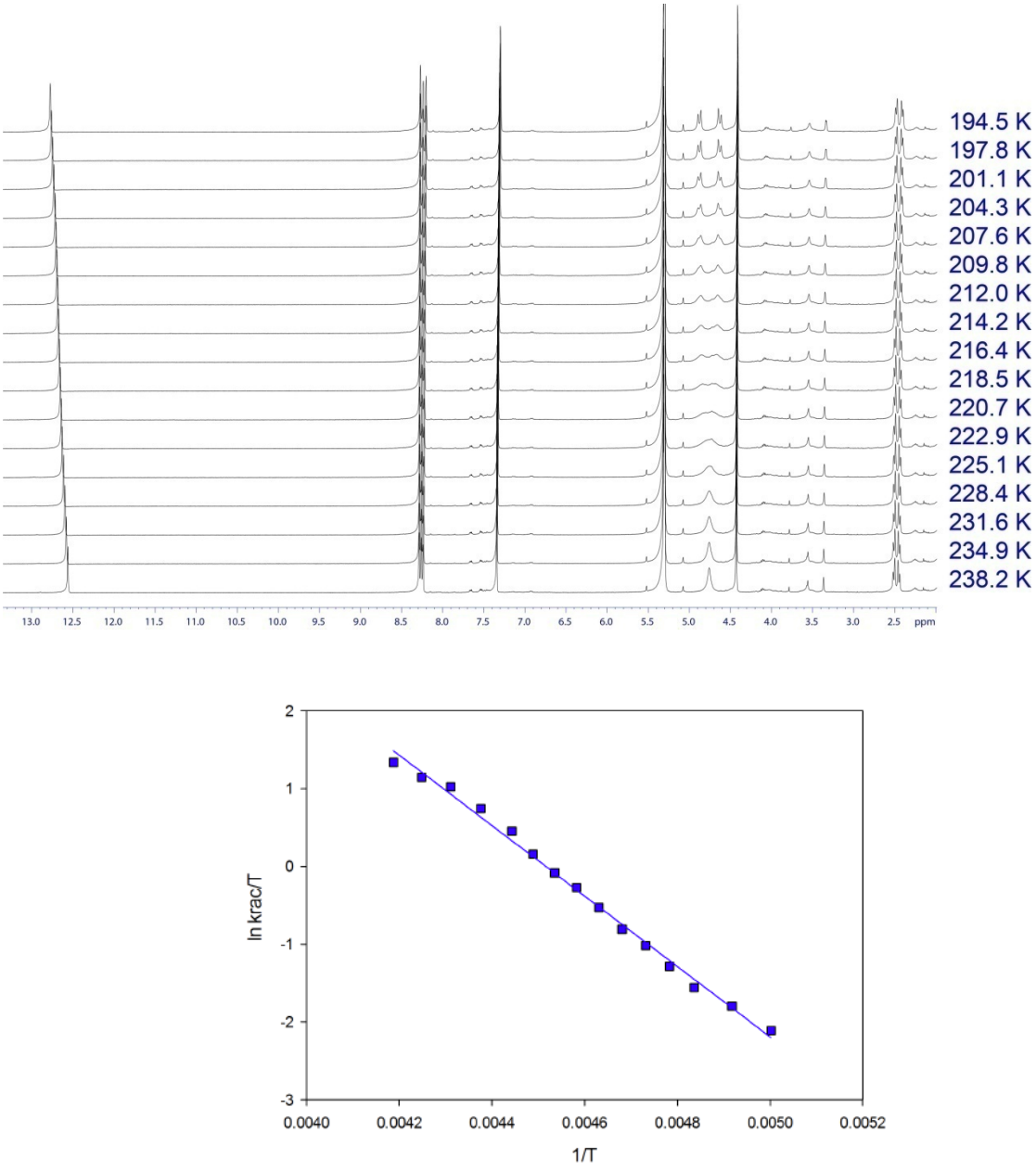

Figure S12. (Top) Variable temperature ^{1}H NMR spectra (400 MHz) of basket **1** (2.5mM)in CD_2Cl_2. (Bottom) The Eyring plot corresponding to the *P*/*M* racemization of the basket for which the rate constant (k_{rac}) was obtained from the classical band-shape analysis (WinDNMR) of $\mathbf{H}_d$ resonances changing from a singlet into an AB quartet.

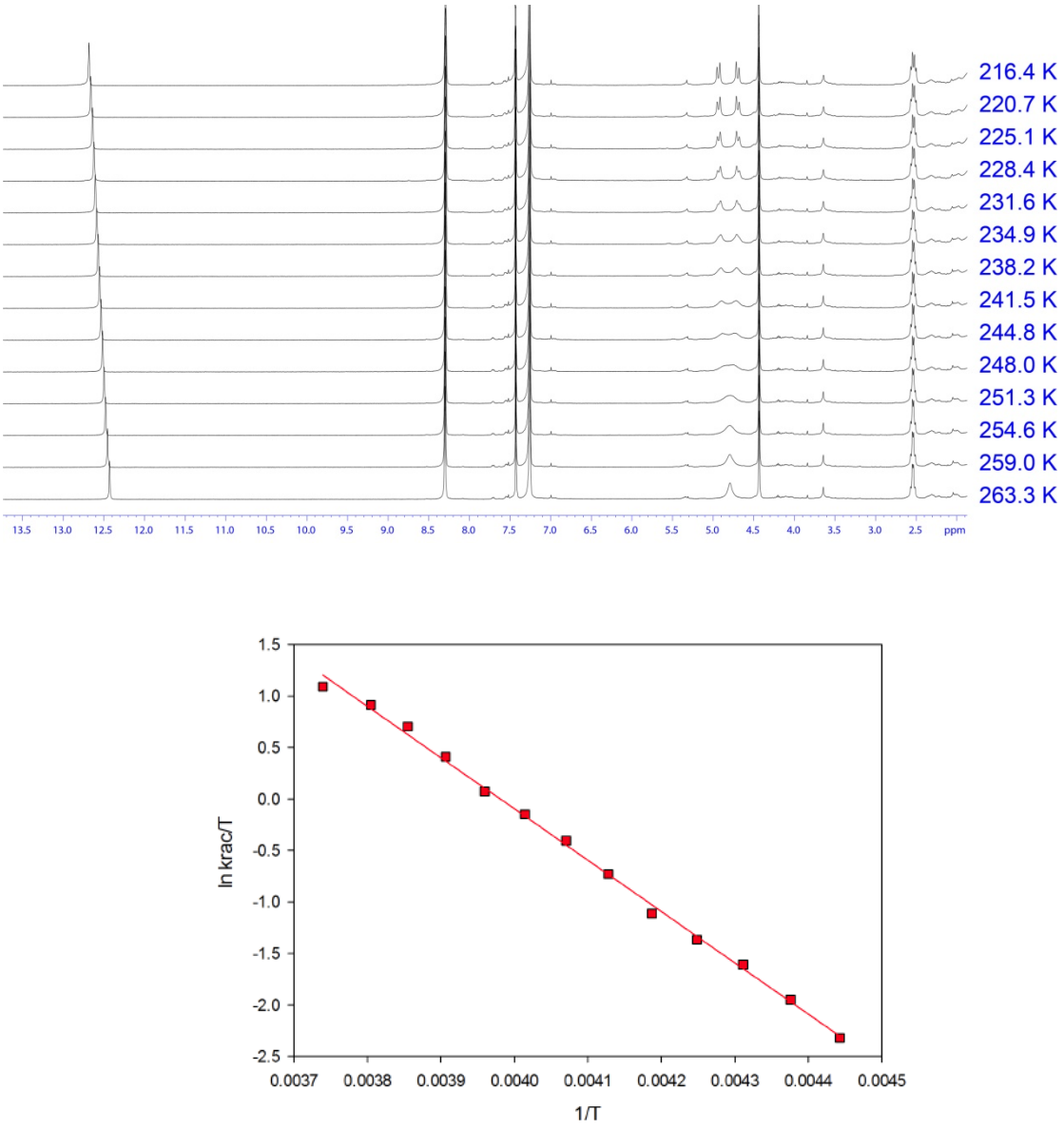

Figure S13.(Top) Variable temperature ^{1}H NMR spectra (400 MHz) of basket **1** (2.0mM) in $CDCl_3$. (Bottom) The Eyring plot corresponding to the *P*/*M* racemization of the basket for which the rate constant (k_{rac}) was obtained from the classical band-shape analysis (WinDNMR) of $\mathbf{H}_d$ resonances changing from a singlet into an AB quartet.

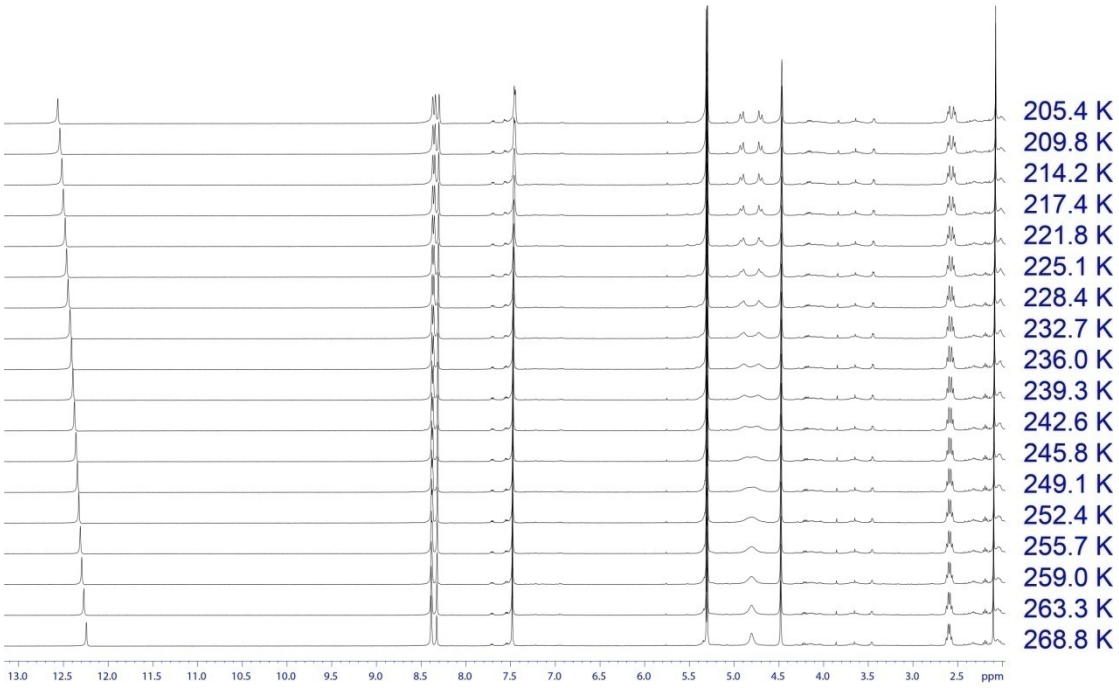

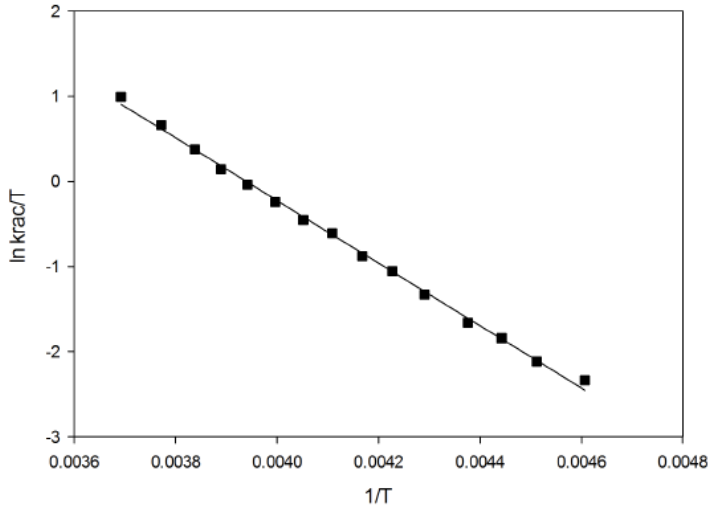

Figure S14. (Top) Variable temperature ^{1}H NMR spectra (400 MHz) of basket **1** (2.0mM) in $CFCl_3/CD_2Cl_2$ = 7:3. (Bottom) The Eyring plot corresponding to the *P*/*M* racemization of the basket for which the rate constant (k_{rac}) was obtained from the classical band-shape analysis (WinDNMR) of $\mathbf{H}_d$ resonances changing from a singlet into an AB quartet.

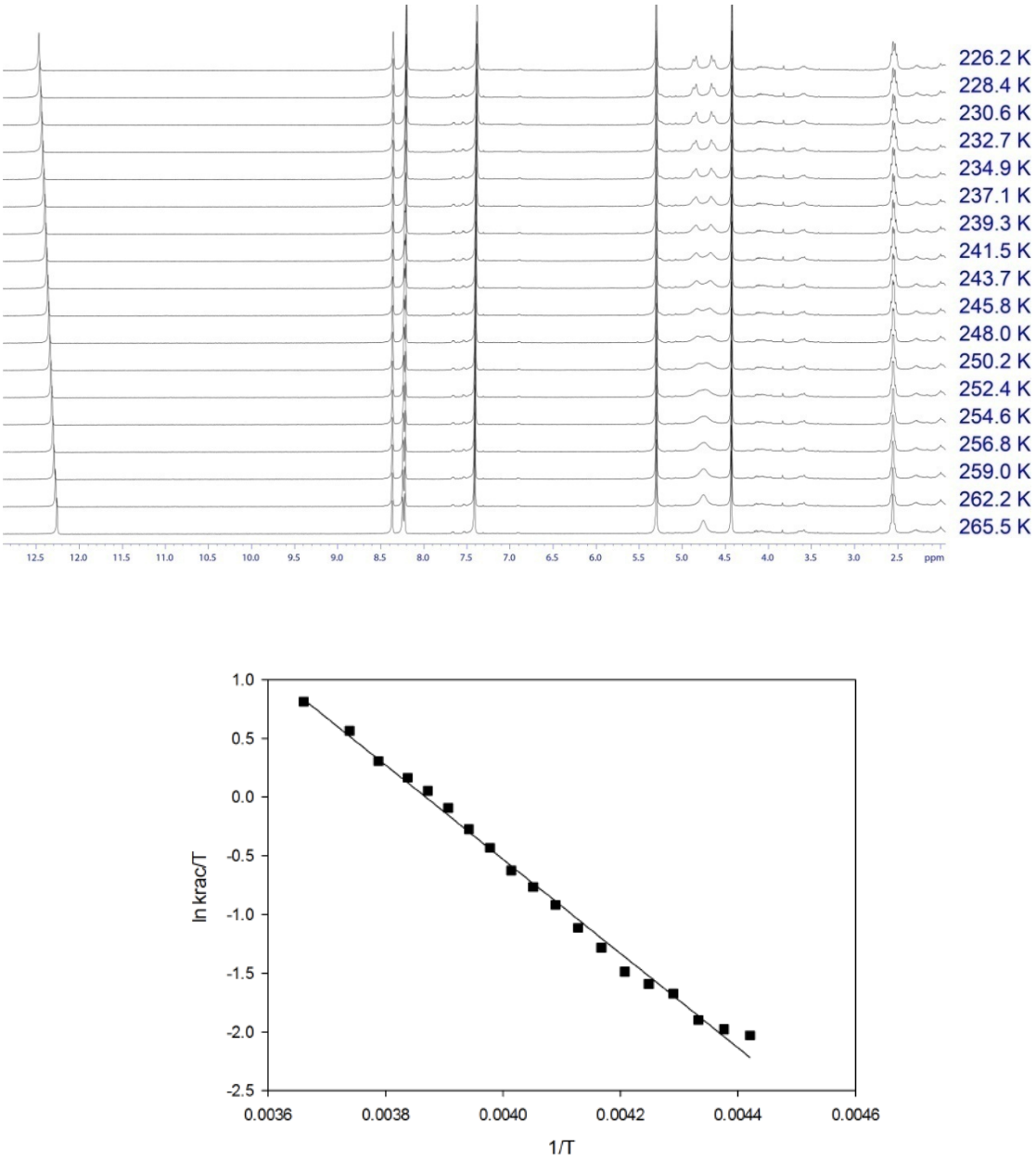

Figure S15. Variable temperature ^{1}H NMR spectra of 2.0mM CCl_4(20% CD_2Cl_2) solution of **1** (400MHz).(Top) Variable temperature ^{1}H NMR spectra (400 MHz) of basket **1** (2.0mM)in CCl_4/CD_2Cl_2 = 8:2. (Bottom) The Eyring plot corresponding to the *P*/*M* racemization of the basket for which the rate constant (k_{rac}) was obtained from the classical band-shape analysis (WinDNMR) of $\mathbf{H}_d$ resonances changing from a singlet into an AB quartet.

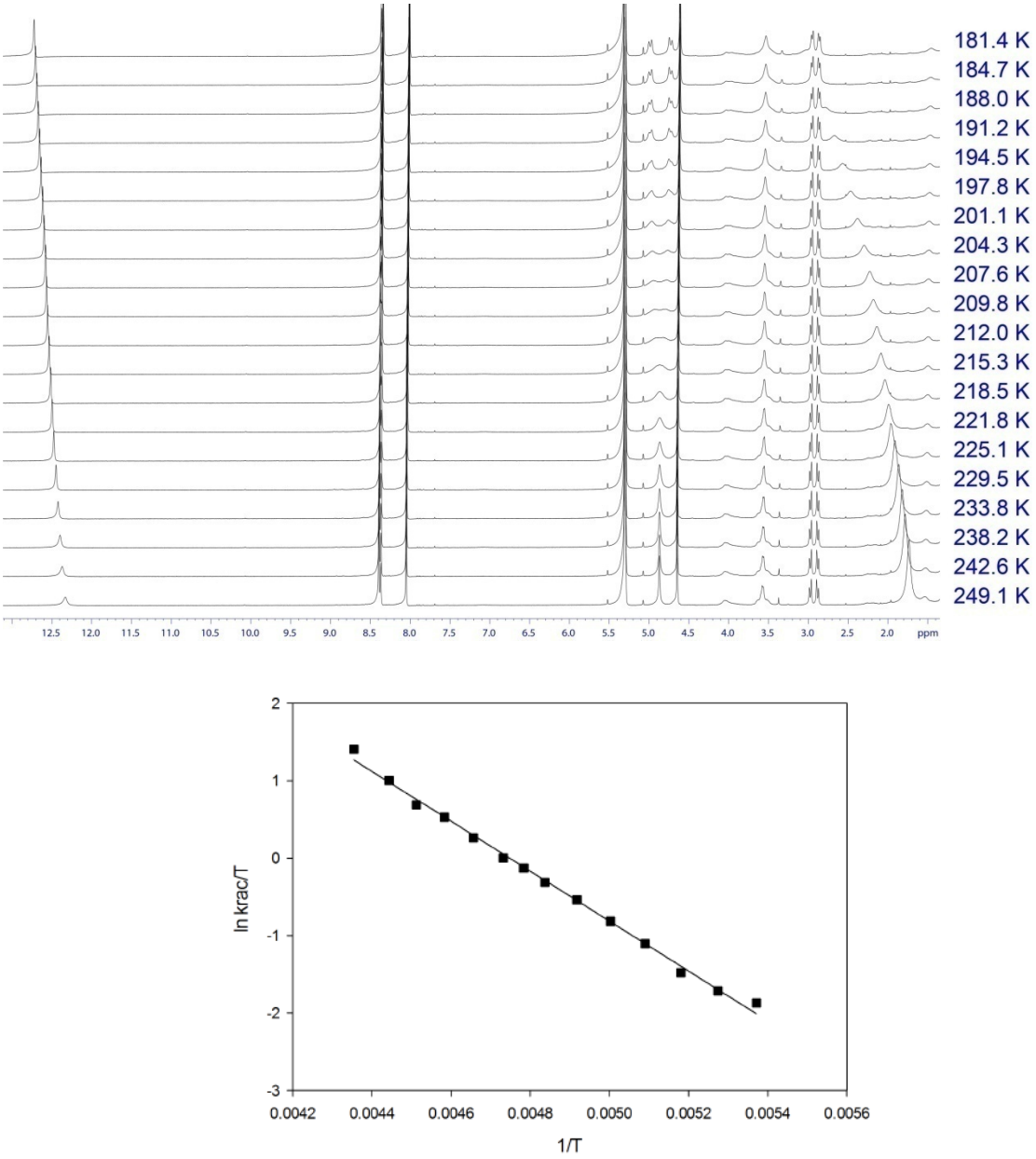

Figure S16. (Top) Variable temperature ^{1}H NMR spectra (400 MHz) of basket **2** (0.5mM) in CD_2Cl_2. (Bottom) The Eyring plot corresponding to the *P*/*M* racemization of the basket for which the rate constant (k_{rac}) was obtained from the classical band-shape analysis (WinDNMR) of $\mathbf{H}_d$ resonances changing from a singlet into an AB quartet.

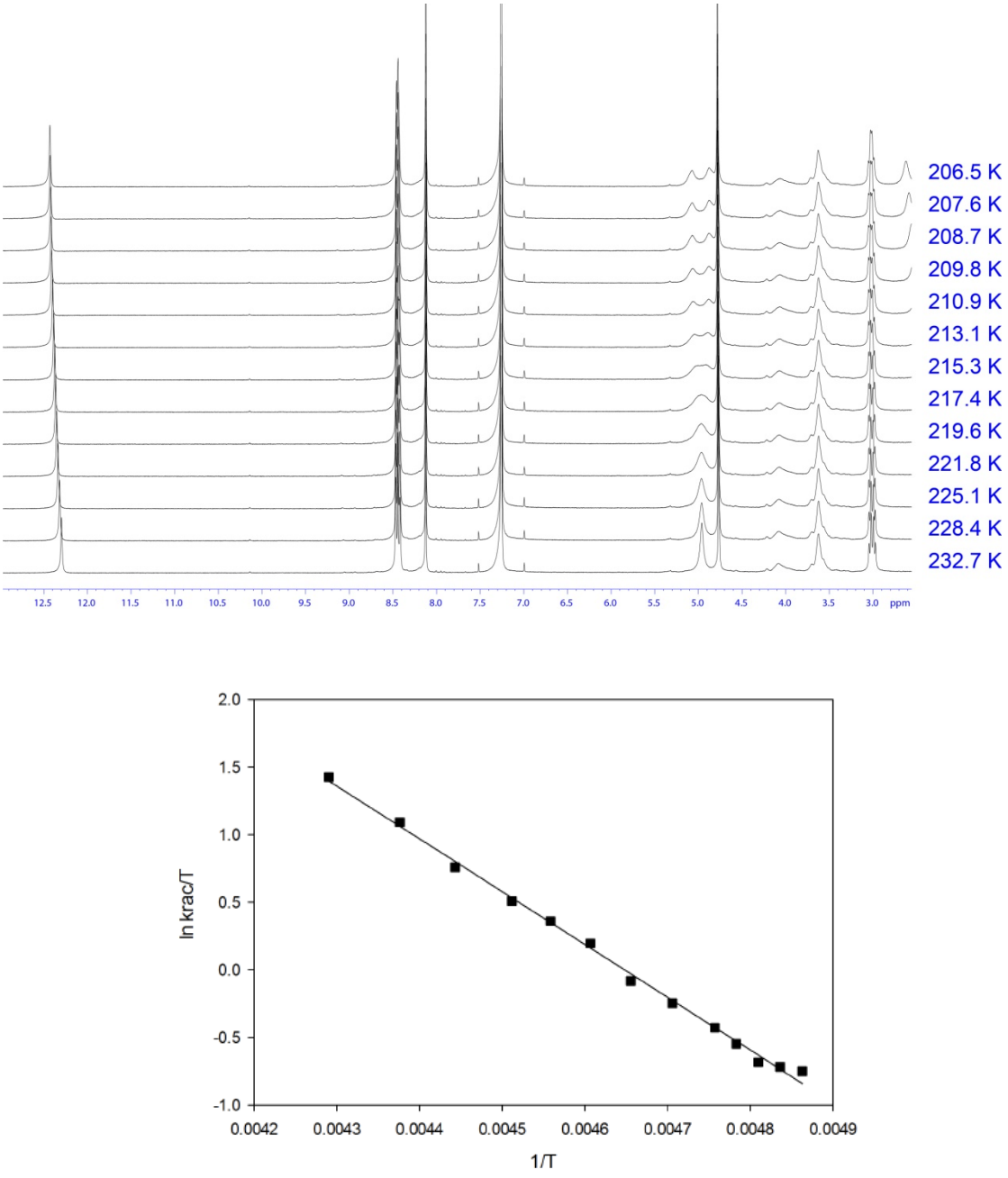

Figure S17. (Top) Variable temperature ^{1}H NMR spectra (400 MHz) of basket **2** (0.5mM) in $CDCl_3$. (Bottom) The Eyring plot corresponding to the *P*/*M* racemization of the basket for which the rate constant (k_{rac}) was obtained from the classical band-shape analysis (WinDNMR) of $\mathbf{H}_d$ resonances changing from a singlet into an AB quartet.

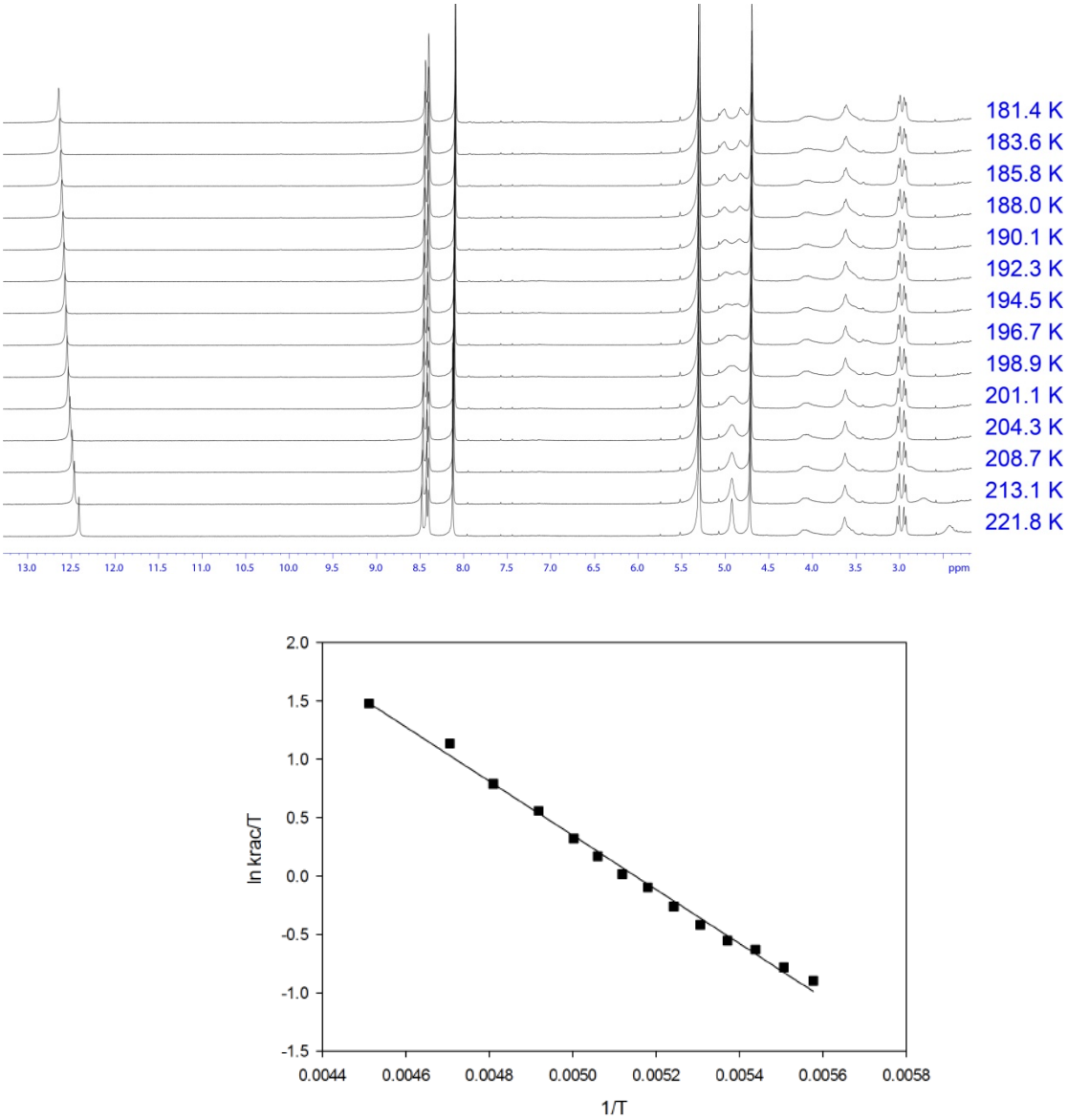

Figure S18. (Top) Variable temperature ^{1}H NMR spectra (400 MHz) of basket **2** (0.5mM) in $CFCl_3/CD_2Cl_2$ = 7:3. (Bottom) The Eyring plot corresponding to the *P*/*M* racemization of the basket for which the rate constant (k_{rac}) was obtained from the classical band-shape analysis (WinDNMR) of $\mathbf{H}_d$ resonances changing from a singlet into an AB quartet.

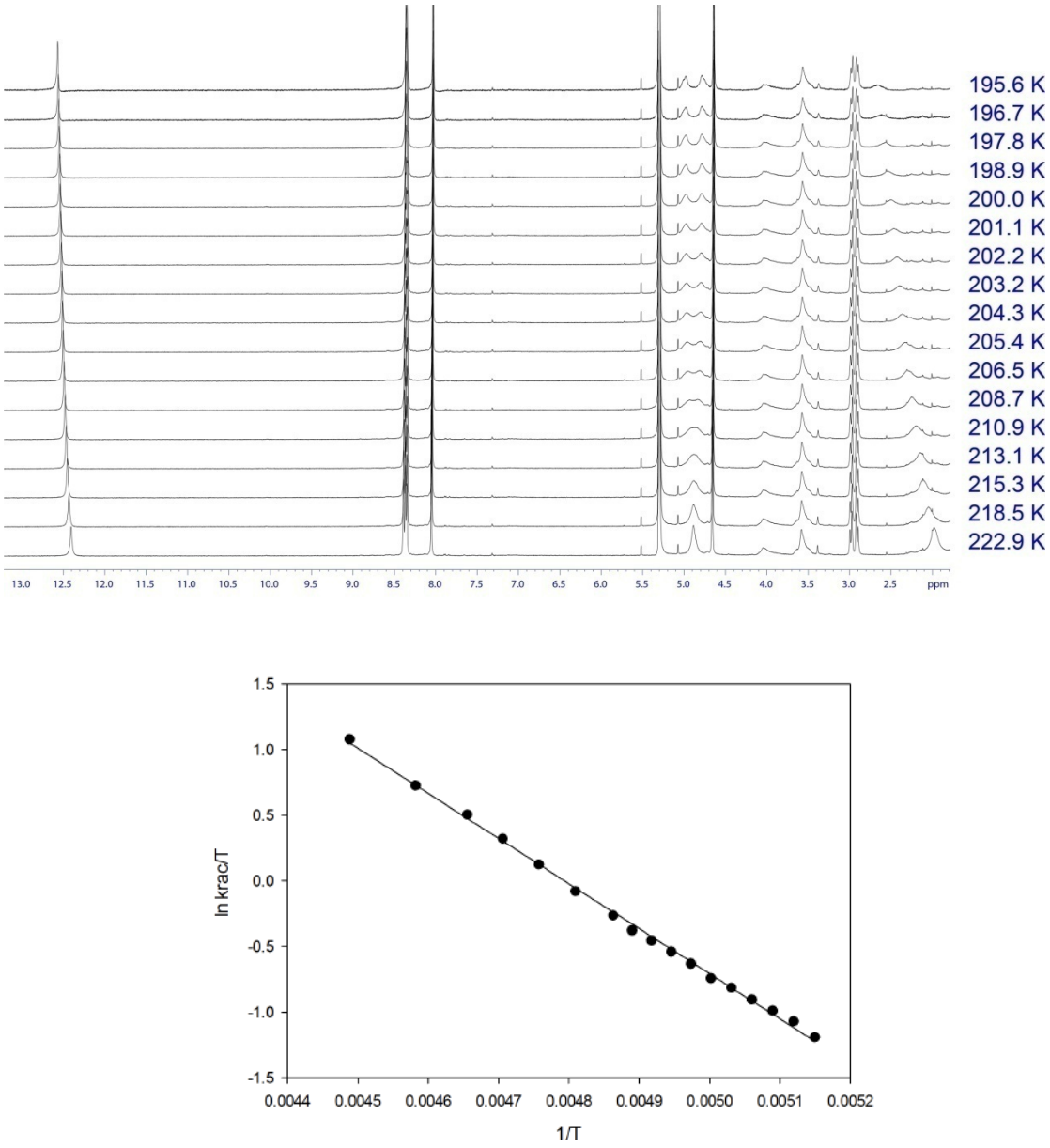

Figure S19. (Top) Variable temperature ^{1}H NMR spectra (400 MHz) of basket **2** (0.5mM) in CCl_4/CD_2Cl_2 = 8:2. (Bottom) The Eyring plot corresponding to the *P*/*M* racemization of the basket for which the rate constant (k_{rac}) was obtained from the classical band-shape analysis (WinDNMR) of $\mathbf{H}_d$ resonances changing from a singlet into an AB quartet.

References

1. Svoboda, J., Schmaderer, H. and König, B. (2008), *Chemistry - A European Journal*, 14: 1854–1865.
2. Goldstein, H. and Merminod, J.-P. (1952), Helvetica ChimicaActa, 35: 1476–1480.
3. Williams, R. L. and Shalaby, S. W. (1973), *J. Heterocyclic Chem*., 10: 891–898.
4. Kobayashi, T.; Kobayashi, S. *Molecules* **2000**, *5*, 1062-1067.
5. Morisawa, Y.; Kataoka, M.; Sakamoto, T.; Saito, F. *Agricultural Biol. Chem.*1976, *40*, 101-105.

Computational Protocol

All basket computations were performed by first optimizing the geometry with the semi-empirical PM6 method followed by single point energy calculations with density functional theory at the B3LYP/6-31+G** level of theory. All computations were performed using Gaussian '09. Single point energy computations (B3LYP/6-31+G**) for the RM_3 movement for both **1** and **1-Me** were optimized with PM6 or B3LYP/6-31G* and comparedwhile their energies were found to be similar so the less expensive PM6 computations were used for all subsequent optimization calculations (Figure S20). Note: some DFT calculations did not converge, but were changing in energy by an insignificant amount (less than 10^{-6}Hartrees).

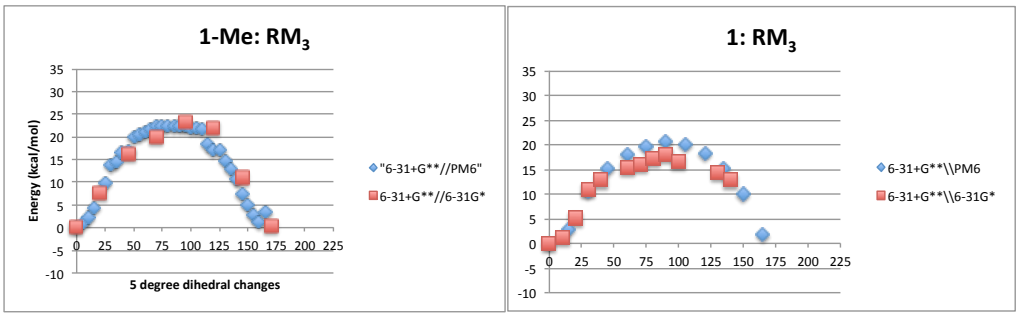

Figure S20. Comparison of Geometry for **1**

Geometries on the graphs below were obtained by first optimizing each of the four baskets to obtain the lowest energy structure. Then, each dihedral angle of interest was changed by 5° increments. For graphs mapping the movement of RM_1, φ_1 was held frozen on the arm moving outward during each optimization. For graphs mapping the movement of RM_2, $\varphi_1$of the arm moving outward and φ_2 of each arm perform the gating motion were held frozen during each optimization.For graphs mapping the movement of RM_3, φ_2 of each arm was held frozen during each optimization. These optimized structures were used as starting structures and the optimizations were performed again until the resulting energy curve pictured on the graph below looked smooth and unchanged (minimum energy path). Then, the geometries obtained by the PM6 optimizations were subjected to SP energy computations at the B3LYP/6-31+G** level of theory. Note: In order to reach the completely inverted end structure of **1** and **2** for RM_2, one of the arms has to move slightly faster (φ_2) than the other. For this to happen, an exact 5° incrementwas not held strict between structures listed at 35° and 40° for **2** and 45° and 50° for **1**. The coordinates for each structure is listed as *structure:#*, where **1**:1 would be the starting structure for 1, **1**:2 is the structure with the specified dihedral moved by 5°, etc.

Basket **1**:

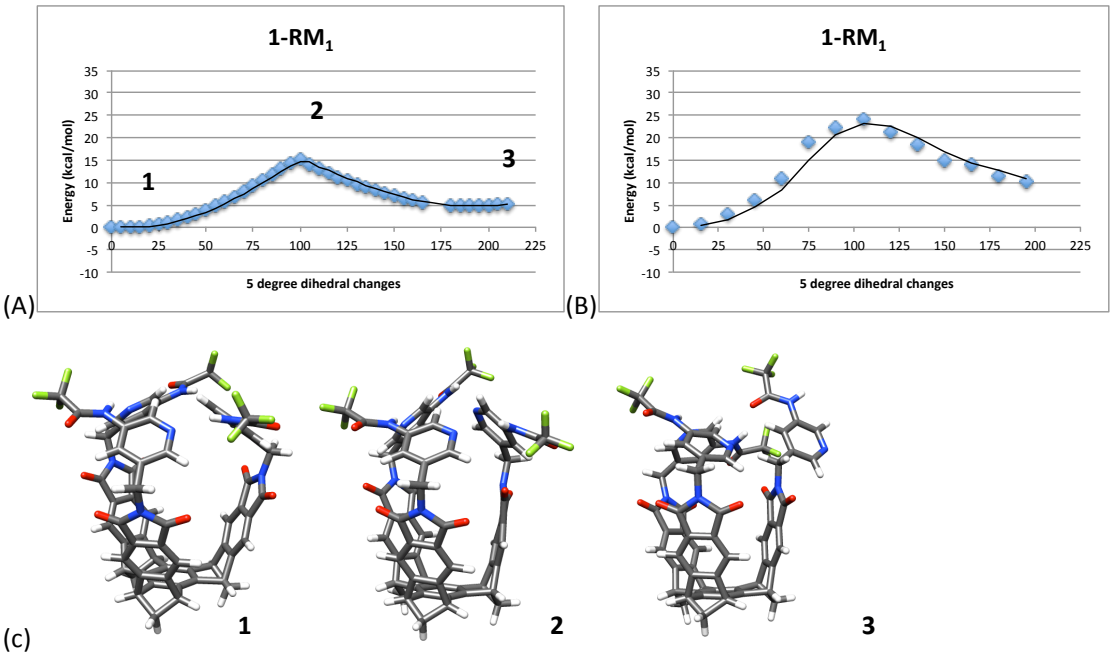

Figure S21. RM_1movement plots of **1** with (a) PM6 (b) B3LYP/6-31+G**//PM6 (c) graphical representation of structures.

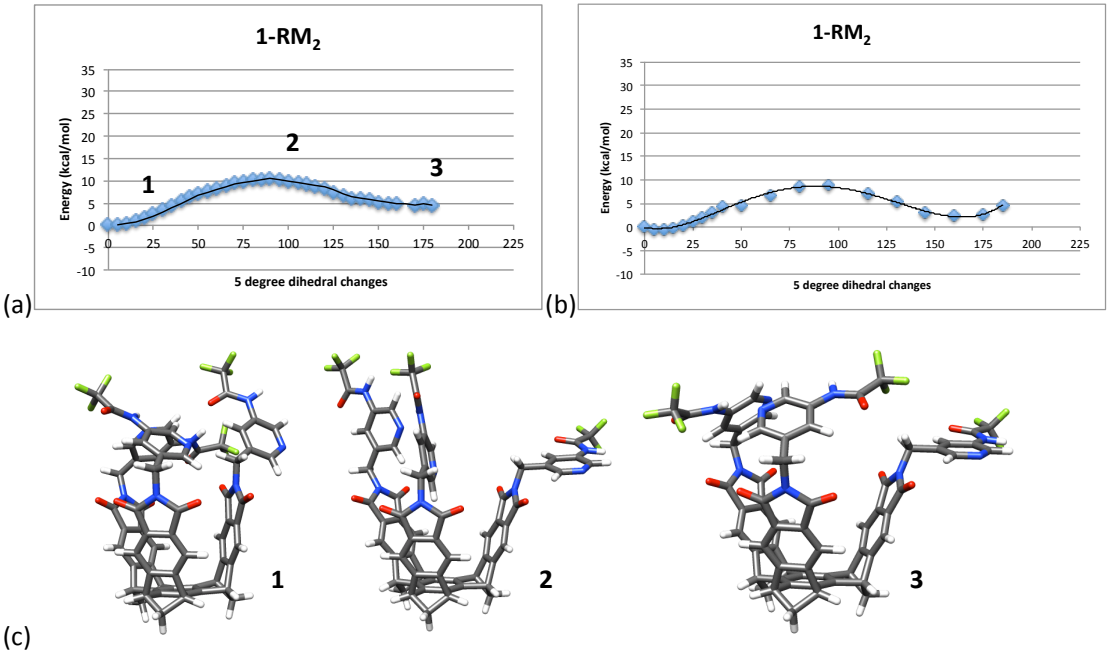

Figure S22. RM_2movement plots of **1** with (a) PM6 (b) B3LYP/6-31+G**//PM6 (c) graphical representation of structures.

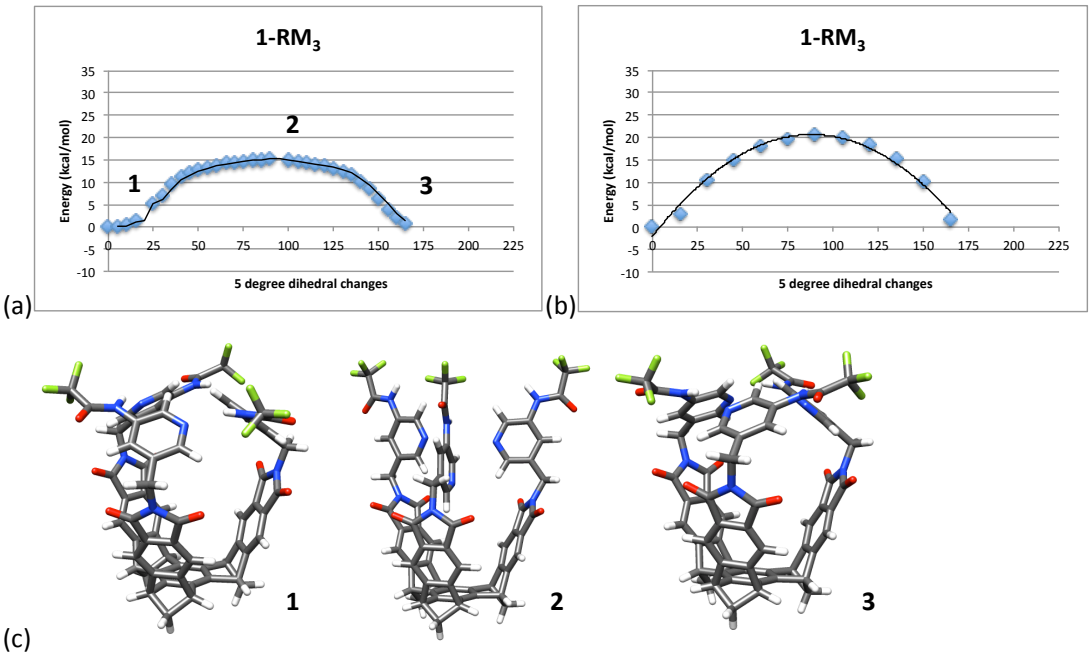

Figure S23. RM_3movement plots of **1** with (a) PM6 (b) B3LYP/6-31+G**//PM6 (c) graphical representation of structures.

Structure **2**:

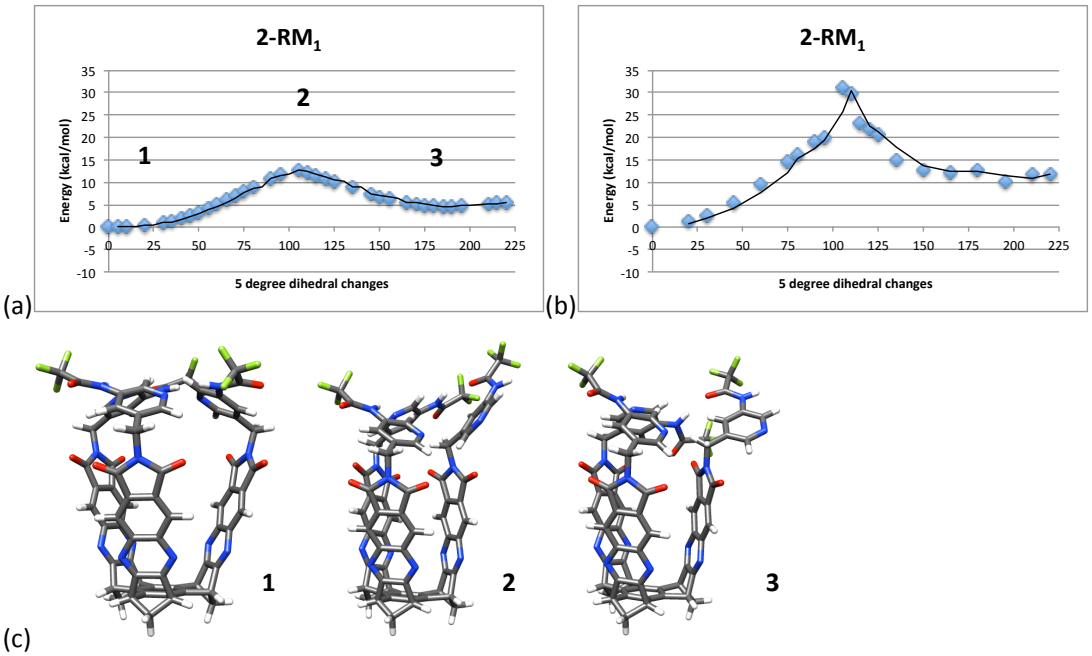

Figure S24. RM_1movement plots of **2** with (a) PM6 (b) B3LYP/6-31+G**//PM6 (c) graphical representation of structures.

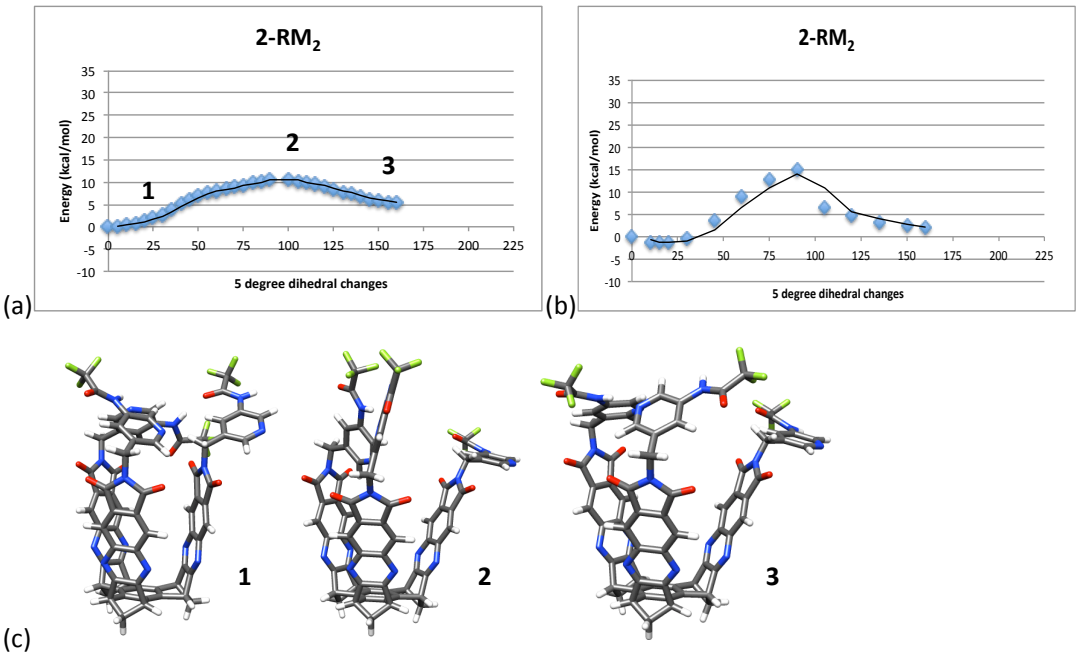

Figure S25. RM_2movement plots of **2** with (a) PM6 (b) B3LYP/6-31+G**//PM6 (c) graphical representation of structures.

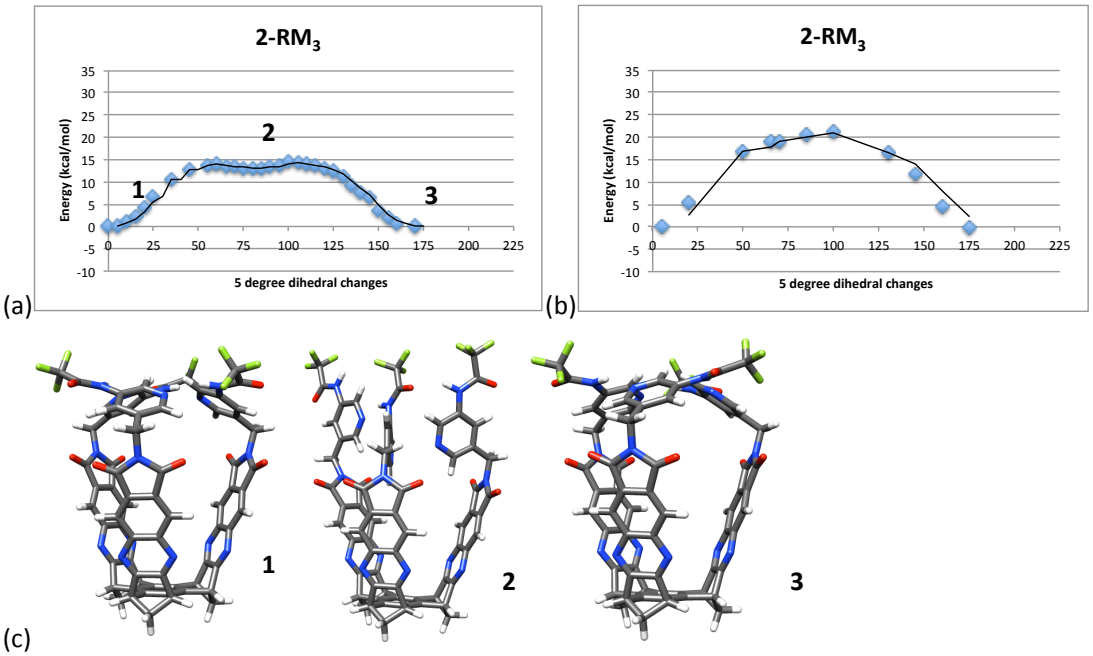

Figure S26. RM_3movement plots of **2** with (a) PM6 (b) B3LYP/6-31+G**//PM6 (c) graphical representation of structures.

Structure **1-Me**:

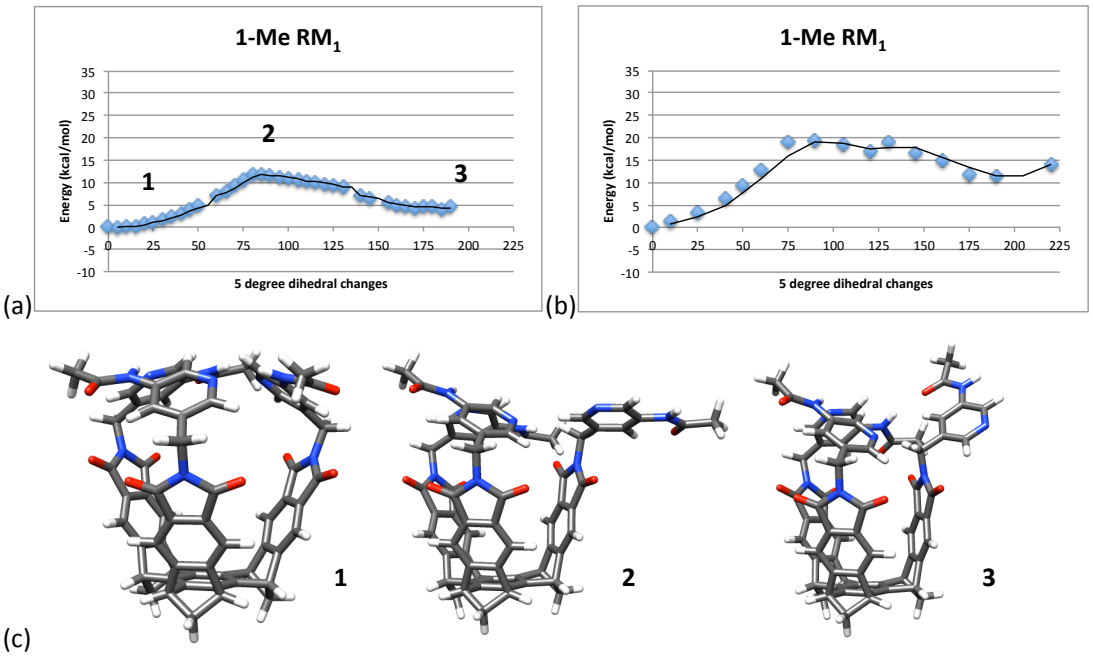

Figure S27. RM_1movement plots of **1-Me** with (a) PM6 (b) B3LYP/6-31+G**//PM6 (c) graphical representation of structures.

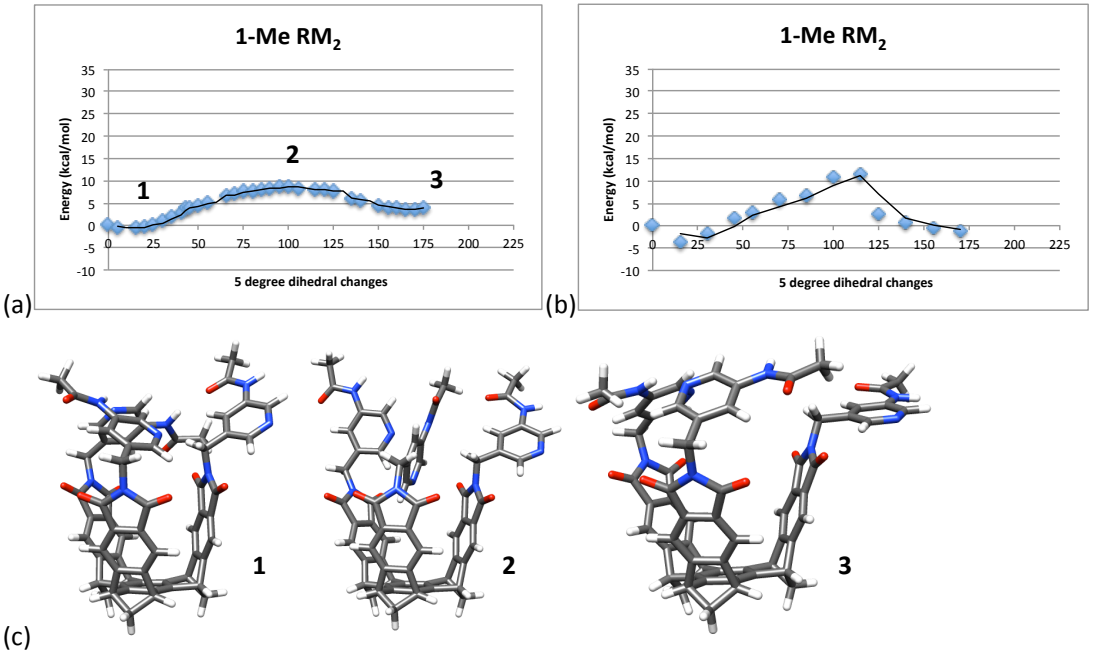

Figure S28. RM_2movement plots of **1-Me** with (a) PM6 (b) B3LYP/6-31+G**//PM6 (c) graphical representation of structures.

(a)

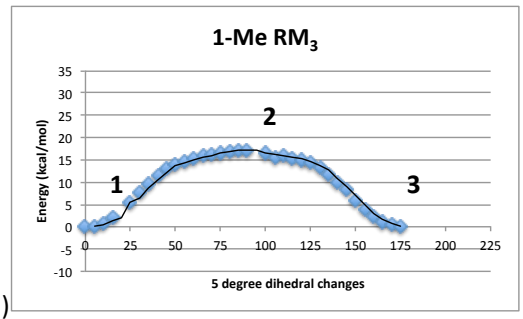

(b)

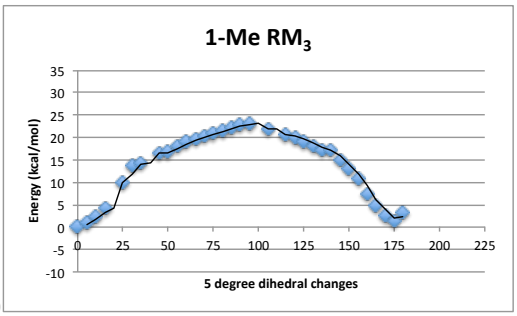

(c)

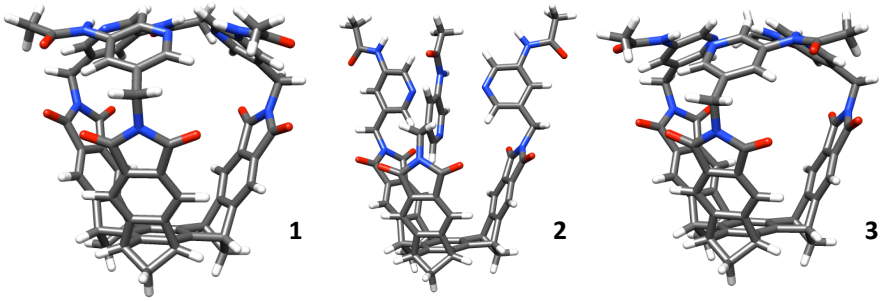

Figure S29. RM_3movement plots of **1-Me** with (a) PM6 (b) B3LYP/6-31+G**//PM6 (c) graphical representation of structures.

Structure 2-Me:

(a)

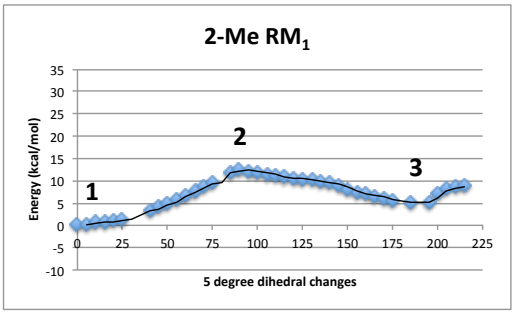

(b)

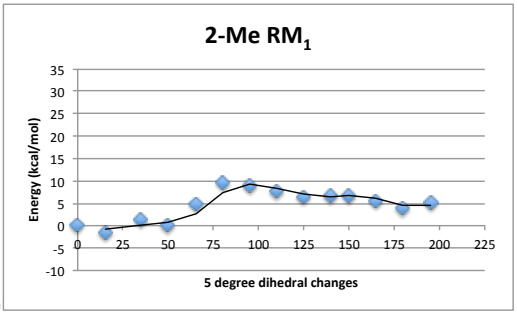

(c)

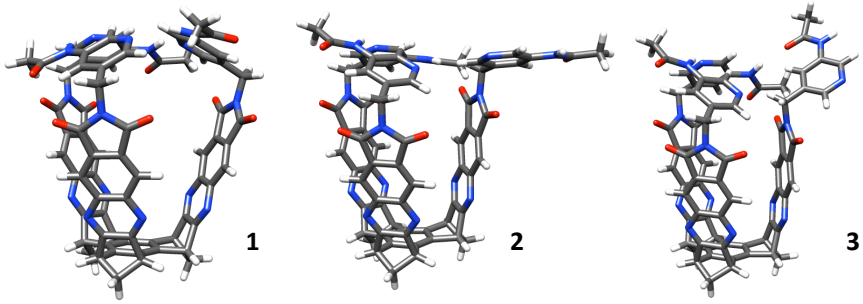

Figure S30. RM_1movement plots of **2-Me** with (a) PM6 (b) B3LYP/6-31+G**//PM6 (c) graphical representation of structures.

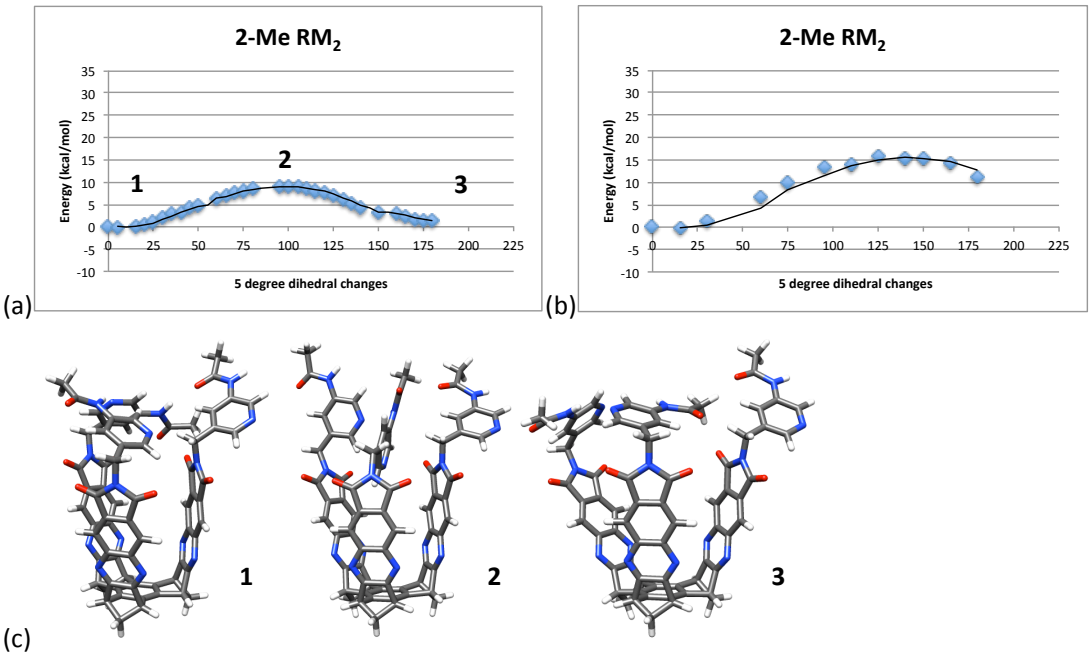

Figure S31. RM_2movement plots of **2-Me** with (a) PM6 (b) B3LYP/6-31+G**//PM6 (c) graphical representation of structures.

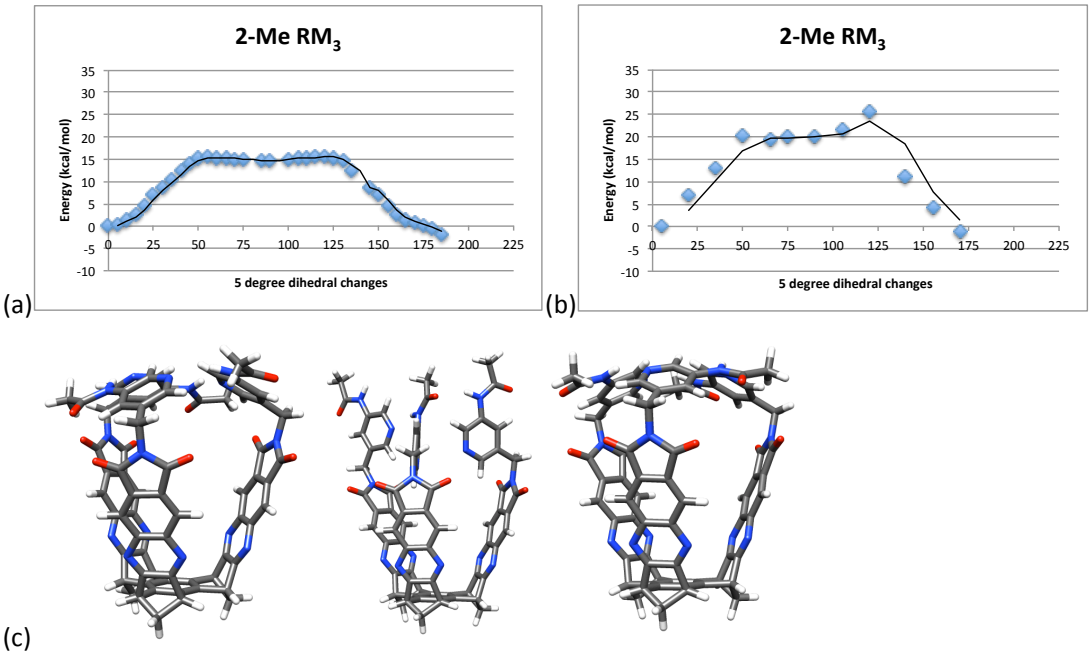

Figure S32. RM_3movement plots of **2-Me** with (a) PM6 (b) B3LYP/6-31+G**//PM6 (c) graphical representation of structures.

	1 - CF_3 basket					
	RM_1 - ϕ_1		RM_3 - ϕ_2		RM_2 - ϕ_2	
	start	finish	start	finish	start	finish
arm1	-83.6	126.7	90.9	-100.1	N/A	N/A
arm2	-81.3	-82.8	86.1	-103.4	112.7	-92.2
arm3	-80.9	-74.5	96.1	-93.8	82.2	-81.9

	2 - CF_3 basket					
	RM_1 - ϕ_1		RM_3 - ϕ_2		RM_2 - ϕ_2	
	start	finish	start	finish	start	finish
arm1	-84.6	128.2	94.3	-93.1	N/A	N/A
arm2	-84.6	-83.2	94.2	-93.2	71.8	-101.5
arm3	-84.6	-78	94.3	-93	112.6	-104.7

	1 - Me basket					
	RM_1 - ϕ_1		RM_3 - ϕ_2		RM_2 - ϕ_2	
	start	finish	start	finish	start	finish
arm1	-79.7	130.1	88.8	-88.8	N/A	N/A
arm2	-81.8	-73.2	88.6	-89.2	91.1	-91.2
arm3	-81.1	-93.9	88.9	-89.7	87.2	-89.9

	2 - Me basket					
	RM_1 - ϕ_1		RM_3 - ϕ_2		RM_2 - ϕ_2	
	start	finish	start	finish	start	finish
arm1	-82.2	118	90.9	-83.5	N/A	N/A
arm2	-92.5	-91.8	90.8	-83.5	92.8	-83.2
arm3	-86.4	-77.9	90.9	-83.6	93.1	-85.5

Table S3.Dihedral Angles – Values listed are in degrees.